Neutron beam enhancement in a reactor beam port

by

Henry Irving Crook, Jr.

A Thesis Submitted to the
Graduate Faculty in Partial Fulfillment of
The Requirements for the Degree of
MASTER OF SCIENCE

Major Subject: Nuclear Engineering

Iowa State University
Ames, Iowa

1972

TABLE OF CONTENTS

INTRODUCTION

Most experimenters doing research with neutron beams use the slow or thermal neutrons which are defined as being those with energies up to approximately 0.4 electron volts. A common source of such neutrons is a research reactor beam port. The reactor beam port is usually designed to allow neutrons from the core or reflector region of the reactor to travel out through the port to the experimental apparatus. A beam obtained in this manner will consist primarily of the radial component of the reactor neutron flux which is incident on the inner end of the beam tube, Figure 1.

Experimenters using a neutron beam generally are only interested in a narrow range of energies, especially if neutron diffraction studies are to be performed. The neutrons with other energies may constitute a serious background problem especially if they are fast neutrons which are far more difficult to shield. Therefore, if the spectrum was modified to increase the percentage of neutrons in the energy region of interest, the beam would be more useful.

There have been instances where the ratio of the thermal nuetron flux at the inner end of a beam port to the thermal neutron flux at the reactor face from that beam port have differed by as much as a factor of 10 for two different reactors [2]. This difference clearly indicates that some additional information is needed in this area.

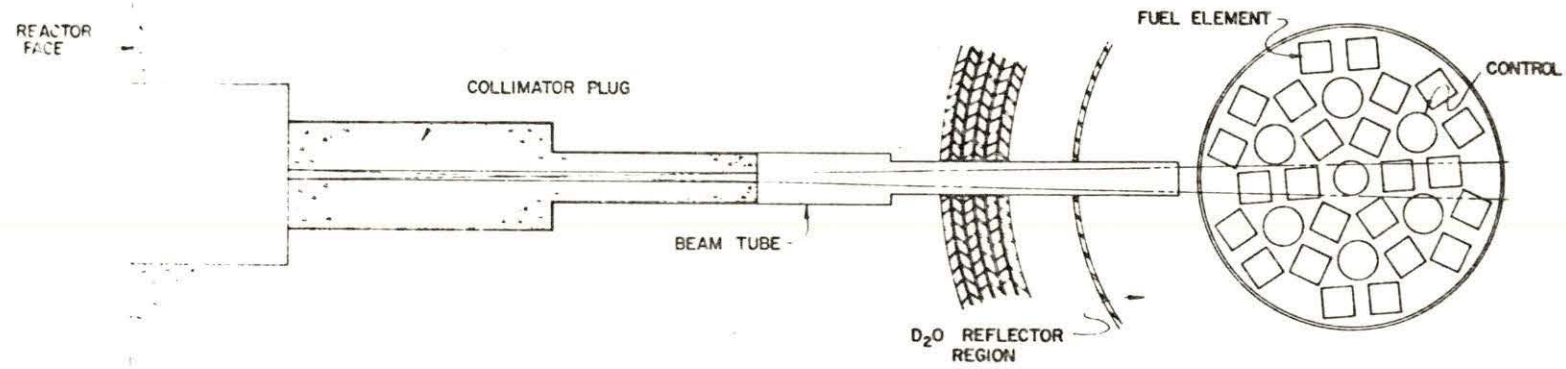

Figure 1. A typical solid angle view of the core and reflector

Experimenters at the CP-5 reactor and Ames Laboratory Research Reactor (ALRR) interested in modifying the neutron beam for their use had indicated they did not know what material to use, how much, or the optimum location for it. When the Mitsubishi double beam neutron diffractometer was to be installed at one of the ALRR beam ports, a literature search to determine how the beam could best be optimized with respect to neutrons of 1 A° wavelength was performed by various groups at Ames Laboratory. Very little information was revealed as a result of their search.

The primary reason for this research was to permit better use of the horizontal beam tubes of research reactors. One objective of the investigation was to measure the slow neutron energy spectrum from a beam port at the Ames Laboratory Research Reactor. A Fermi type slow neutron chopper [12] with an electronic time of flight analyzer was used to determine the slow neutron energy spectra. The effect of the scattering material position with respect to the reactor core and reflector, the effects of the amount and type of material used upon energy spectra, and the effects of total neutron current and cadmium ratio were investigated. Those materials examined were: graphite, beryllium oxide and beryllium metal.

REVIEW OF LITERATURE

A small number of experiments to modify reactor beams have been described in the literature. The general outline of those studied which pertain to this research is presented here.

A method for reducing the fast neutron flux in the spectrometer beam ports of a light water pool reactor has been investigated experimentally by Bullock, Daniels, and King [3]. The experiment consisted of installing a heavy water tank adjacent to the reactor core in a position which effectively converted two beam ports from a radial geometry to a tangential arrangement with a heavy water source region. The resulting measurements were compared with identical measurements taken from the graphite reflected core. The results showed that the D_2O tank increased the ratio of desired neutron energies to background at the crystal spectrometer by a factor of 2.8 and at the mechanical monochromator by 4.75. These factors included a thermal flux increase of 1.8 at both beam ports. For experiments with a signal to background ratio of less than 2, the beam produced with the D_2O tank resulted in better counting statistics than could be obtained by doubling the reactor power level.

James and Meneley [6] described the neutron flux distribution in a horizontal graphite thermal column with a short vertical stub near the end remote from the neutron source. By introducing large voids in the column and stub they showed

that the spatial distribution of flux at both vertical and horizontal access ports may be adjusted and, if desired, made symmetrical. At the same time the magnitude of the flux at both faces had greatly increased over that for a similar solid column, by factors of up to 80.

The energy spectrum for a beam of neutrons from the Australian High-Flux Reactor, HIFAR, was determined by Sabine, Browne, and Symonds [10]. The neutrons in the beam were taken from a point in the heavy water moderator 9.5 inches from the edge of the reactor core. The mixed energy neutron flux emerging at the face of the reactor shield was 2×10^8 n/cm^2-sec. for a reactor power of 10 megawatts. Crystal spectrometry and activation analysis techniques were used to determine the energy spectra. The corrected differential neutron distribution as a function of velocity was approximately Maxwellian in shape, and corresponded to a neutron temperature of $388 \pm 6°K$. This temperature was about 70°C above the moderator temperature.

During the design stages of the Brookhaven National Laboratory's High-Flux Beam Reactor an experiment was conducted by H. Kouts [7] to provide neutron beams that were tailored to the requirements of individual experiments. The experiment consisted of a mock-up vessel and core arrangement with reentrant beam tubes at various angular positions with respect to the core and reflector. The distance the beam tubes penetrated the reflector region was variable. Each beam

was designed to emphasize some region of the neutron energy spectrum with an associated reduction in the emission of neutrons of unwanted energies, and of gamma rays. In his conclusions, Kouts pointed out that since his program had to be completed in accordance with the design schedules of the reactor a thorough study of the properties of experimental facilities was prevented. Kouts stated that an adequate optimization was realized. The results suggested that research reactors in the future could profit from thorough experimental study of the geometric considerations of beam ports during the design stage.

In discussions with experimenters, some indicated that they had done some minor investigations in the area of beam enhancement which was not published due to insufficient results. Thus the experimenter was more interested in obtaining results than improving the quality of his beam per se, and consequently, he would spend only a small part of his time improving the beam.

THEORY

In a heavy water reactor a considerable portion of the neutron moderation occurs in the reflector region. If the beam tube is air-filled (which is usually the case) then essentially none of the neutrons from the reflector region will be added to the beam that leaves the reactor, since there is nothing in the beam tube to scatter the neutrons.

Typical thermal and fast neutron flux distributions in a heavy water reactor are illustrated in Figure 2, [1]. The distributions give the energy averaged neutron flux as a function of radial position. The flux is nonisotropic as can be seen by the large radial gradient in Figure 2.

With an air-filled reentrant beam tube, those components of the flux not parallel to the beam tube will not contribute to the neutron beam exiting the beam port. With a scattering material replacing the void (air) in the inner end of the tube, scattering and moderation will occur; neutrons traveling other than parallel to the tube are scattered in the exit direction.

It is apparent that this scattering material will attenuate the radial (or parallel) flux component. The thermal flux in Figure 2 is the total flux at that position. However, the component which is parallel to the beam tube axis (Figure 3) will be only a fraction of the total. Therefore, appropriate additions of scattering material could add more neutrons to the beam than are scattered out. This would result in a net

Figure 2. Radial neutron flux distribution of JRR-II as computed using two-group diffusion theory

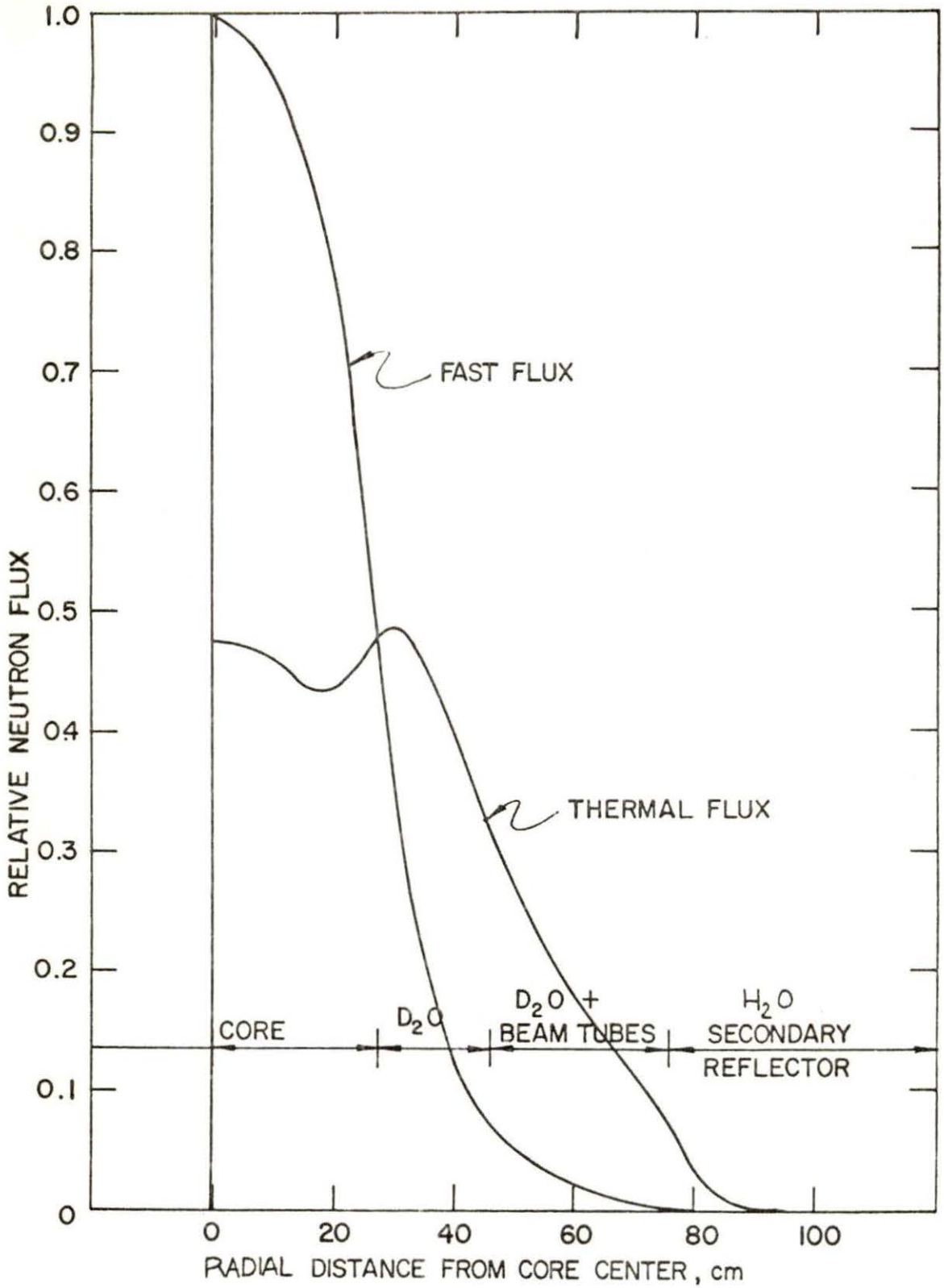
1.0
0.9
0.8
0.7
0.6
0.5
0.4
0.3
0.2
0.1
0
RELATIVE NEUTRON FLUX
FAST FLUX
THERMAL FLUX
CORE
D2O
D2O + BEAM TUBES
H2O SECONDARY REFLECTOR
0
20
40
60
80
100
RADIAL DISTANCE FROM CORE CENTER, cm

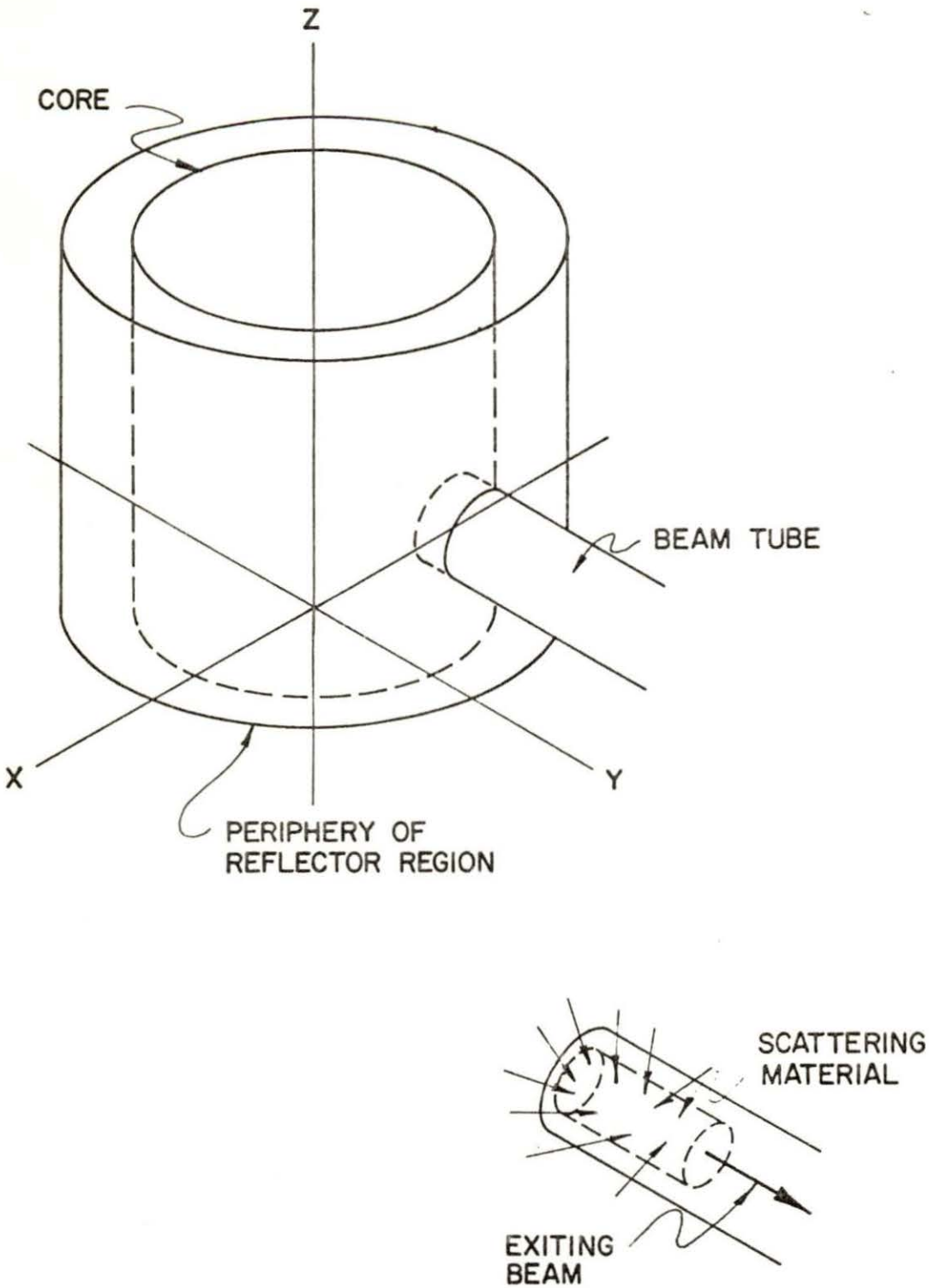

Figure 3. Sketch of reactor core and reflector with beam tube

increase in the total current out of the beam port. One would expect the above to be especially true near the thermal flux peak illustrated in Figure 2. If the thermal neutron current is not increased, but remains approximately the same with an addition of scattering material, then an increase in cadmium ratio should be observed which would be beneficial.

As the amount of scattering material is increased in the axial direction of the beam tube, a point will be reached where the addition (due to the initially non-parallel components and the increased cadmium ratio) produces an increase that is balanced by the radial loss caused by scattering. One purpose of this experiment was to determine this "point" of diminishing return.

While it is obviously desirable for those materials used to have a high scattering cross-section, other considerations must also be made with respect to the materials effect upon the resultant neutron energy spectrum. A material with low absorption cross-section is necessary since absorption reduces not only total neutron flux, but distorts the flux since absorbers which obey a 1/v law preferentially absorb the lower energy neutrons. Thus it would act as a filter as well as a scattering medium. The temperature at which the material operates will also effect the resultant spectrum to a lesser degree. Also, somewhat more practical considerations such as susceptibility to radiation damage and certain mechanical

properties should be present.

The slow neutron energy as observed are expected to approximate a Maxwell-Boltzman distribution of vN(E) vs E, where N(E) is the relative neutron density and v is the neutron speed. The spectra will be hardened due to the presence of fuel, fission products, structural and control materials. Also, hardening will result from an increased population of higher energy neutrons which were produced in fission reactions and are being slowed down by the moderator. The full theoretical energy range of zero to infinity will not be realized due to limitations in experimental equipment. However, to a first order approximation the characteristics of a Maxwell-Boltzmann distribution are expected to be valid. Those characteristics are: 1) the neutron energy corresponding to the most probable energy of the distribution is E_o=kT, 2) the average neutron energy is $\bar{E}$ = 2kT, where T is the neutron temperature (E_o/k) of the Maxwellian distribution corresponding to the most probable neutron energy E_o.

EXPERIMENTAL PROCEDURE

Experimental procedure will be given in two parts. Part A will deal with the equipment and materials. Part B deals with the procedures used in the measurements.

Part A. Equipment

A four inch inner diameter beam port at face number 4 of the ALRR was used for this study (Figure 4). A shielding plug, which had been originally designed for another experiment, had its geometrical arrangement and many of the components fixed. A 0.850 inch O.D. by 0.020 inch wall aluminum tube 49 inches long was extended from the inner end of the shielding plug to the region of interest near the core. Aluminum was used and the tube wall was made very thin to minimize interference with the experiment. The aluminum tube held the material to be tested. The collimator used to define the beam had a 3/8 inch inside diameter and filled the outer fifty-two inch length of the shielding plug (Figure 4). Various tools were designed and fabricated to insert and remove the materials from the core and reflector region.

The distance from the inner end of the beam tube to the outer face of the plug was 100 inches. The minimum nominal distance from the edge of the reactor core to the material tested was approximately three inches. The outer diameter of the material tested was 0.790 inches with varying lengths up to approximately ten inches.

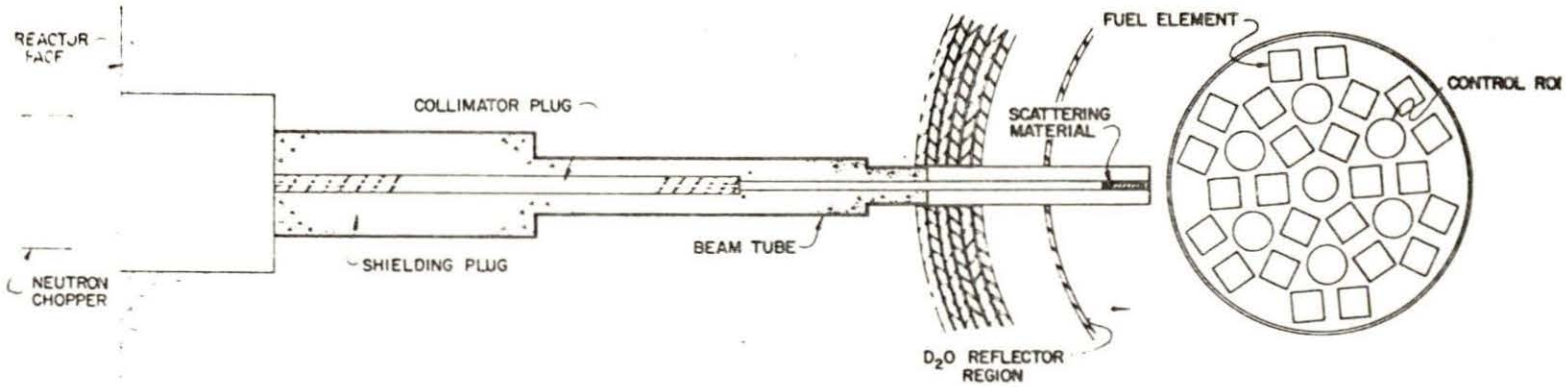

Figure 4. Cross section view showing location of scattering material, core, reflector, collimator and beam tube used in the experiment

To determine the effect of moderating material on the slow neutron energy spectrum, a means of measuring the energy spectrum was needed. A time-of-flight technique was used to determine the slow neutron energy spectrum. The term "time-of-flight" simply means that a burst of polyenergetic neutrons was allowed to start down a flight path at time t_0, and the times were recorded when successive neutrons reach a detector at the end of the flight path. The longer the time interval, the slower the neutrons in that group. A Fermi-type flat slit slow neutron chopper [12] was used to produce the "burst" of polyenergetic neutrons. A neutron chopper like the one shown in Figure 5 is a device which produces pulses of neutrons. The device "chopped" off portions of a collimated neutron beam allowing neutrons to pass during very short intervals of time. A time-of-flight analyzer was an electronic device used to record the number of neutrons which reached the detector during successive time intervals. When the neutron spectrum was being measured the chopper opened at time t_0 and a start pulse was fed to the time-of-flight analyzer (Figure 6). The analyzer then recorded the number of neutrons reaching the detector in successive time intervals and presented them as a time spectrum of the neutron beam. Time-of-flight techniques have high data accumulation rates because of their concurrent energy (i.e., velocity) analysis of all neutrons in the burst.

When deciding which materials to test, consideration was

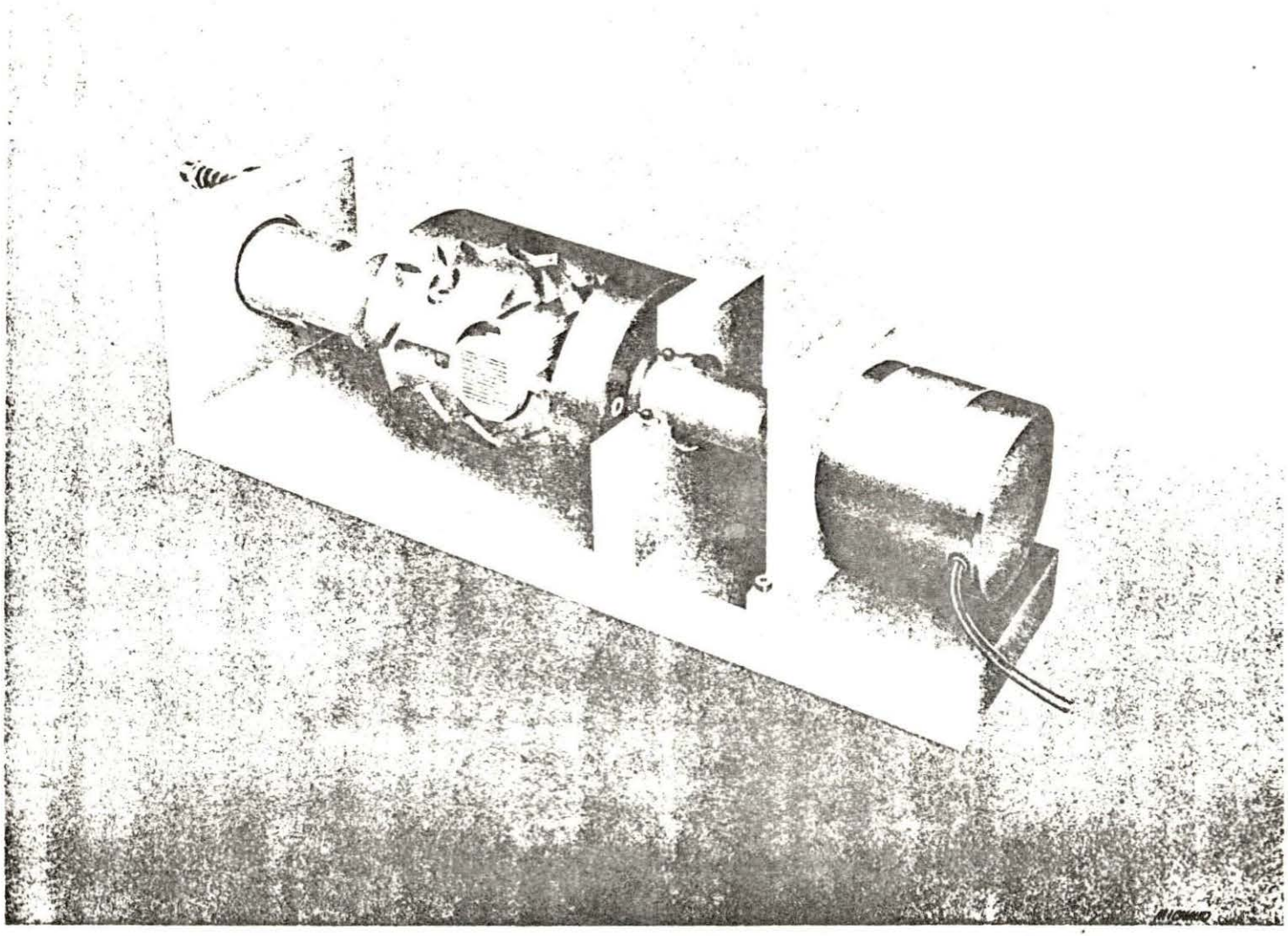

Figure 5. Artist's concept of chopper

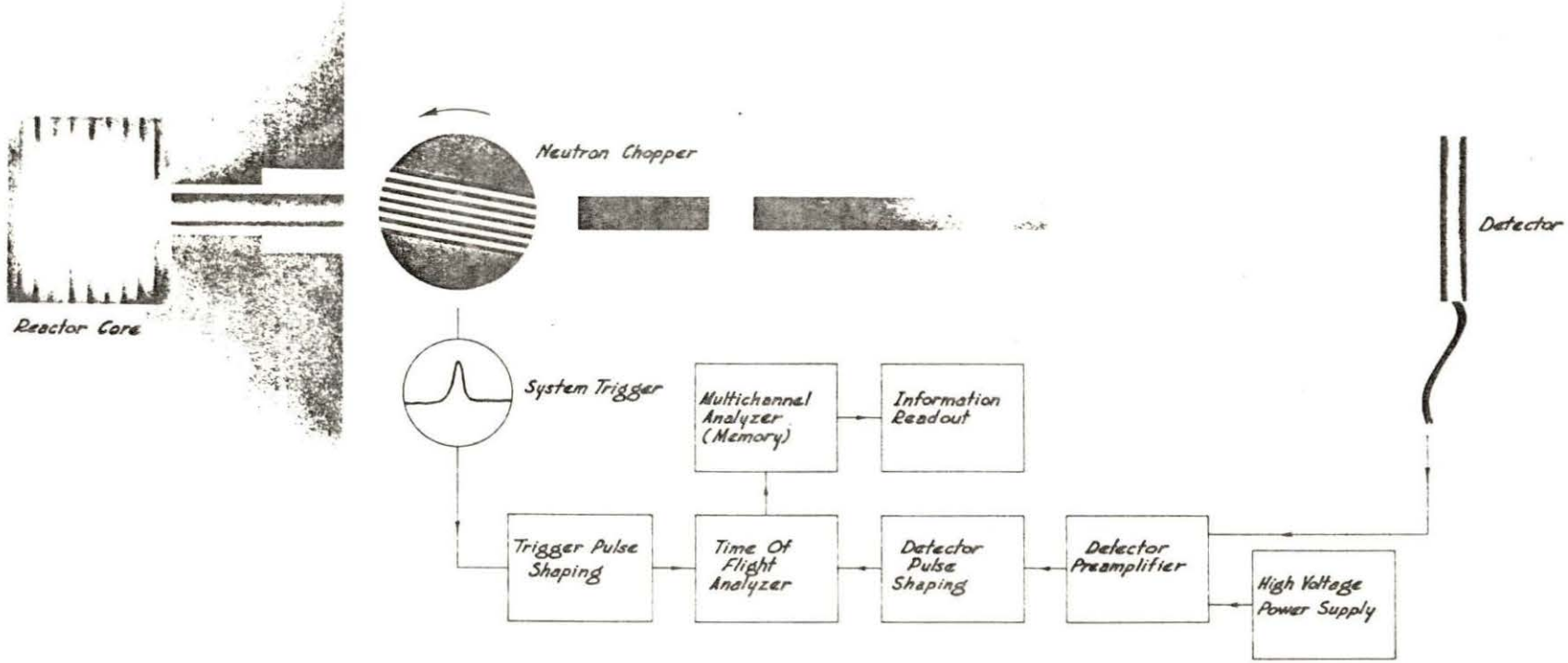

Figure 6. Block diagram of the time-of-flight system used to determine the neutron energy spectrum

given to availability of materials, the compatibility of each with experimental apparatus, and the reasons presented in Theory. Therefore, the materials selected were graphite, beryllium oxide and beryllium metal.

It had been anticipated that the effects of light water and a mixture of 10% light water/90% heavy water, would be investigated. The design of the plug used was such that it proved impossible to circulate a liquid into the region of interest. Therefore, it would be necessary to encapsulate the liquid and insert it in the same manner as previously described. Capsules were designed and fabricated for this purpose. However, upon pre-irradiation testing of the capsules to 500°F pinhole leaks occurred. In one instance the capsule showed signs of bulging before the weld failed. Moreover, several unsatisfactory attempts were made to obtain a tight capsule which would withstand the pressure. This portion of the experiment was finally abandoned as being unsafe for use in the reactor.

Since the neutron beam was attenuated approximately 5% per meter of traversed air, a flight tube (Figure 7) was designed and fabricated which could be evacuated or filled with helium. Another reason for the flight tube was the selective scattering in air which may have caused changes in the spectrum, since the cross sections of oxygen and nitrogen were not constant in the region of energies observed. A change in the

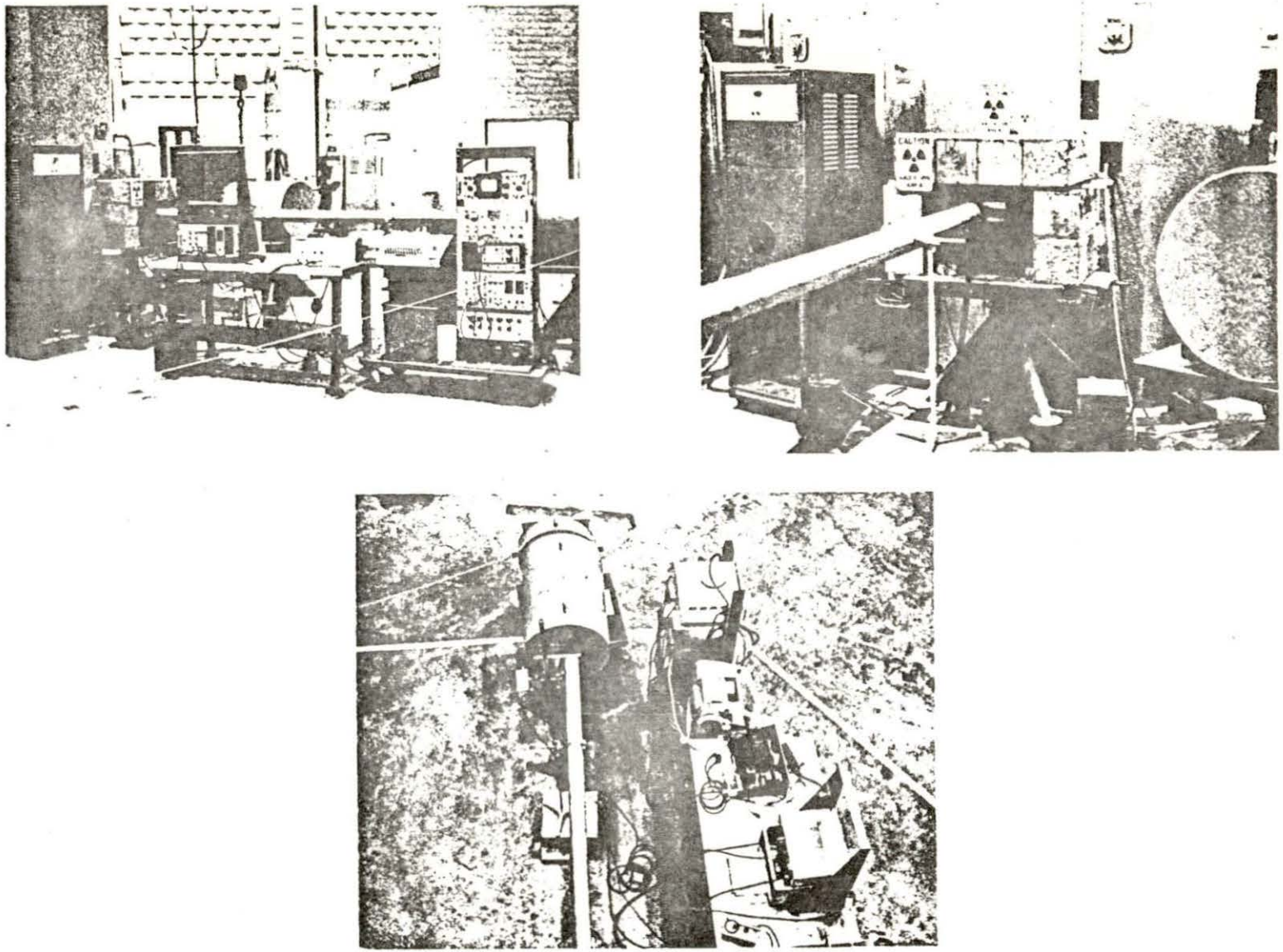

Figure 7. The experimental equipment external to the reactor

total cross section of air on the order of 25% is illustrated in BNL-325 for the energy region of interest here.

With larger amounts of material being tested, the beam intensity was significantly decreased so that longer accumulation times were required. With the addition of the evacuated flight tube, the time required to accumulate the desired data decreased by more than 15%. Vacuum in the flight tube was maintained with a conventional roughing pump.

Part B. Procedures

An initial test run of the experimental equipment was performed to obtain an unmodified slow neutron energy spectrum from a typical beam hole. The previously mentioned four-inch beam port at face number four of the ALLR was used. The chopper was aligned with the collimated gamma beam by the aid of a portable gamma detector. Shielding for neutrons scattered by the chopper, was placed around the chopper. It was soon observed that the neutron scatter problem from the chopper was too great. The 3/8 inch inner diameter beam from the collimator was decreased to a 3/16 inch inner diameter beam by the insertion of a stainless steel tube. Thus the background of fast neutrons was reduced to a tolerable level for personnel in the area. The smaller cross sectional area produced by the modified collimator decreased the beam intensity fourfold; however, it proved to be no great problem since there was sufficient time to accumulate data between reactor shutdowns.

The start pulse from the chopper (Figure 6) was calibrated and modified electronically, as outlined below, to provide the proper input to the time of flight analyzer. In order to calibrate the chopper start pulse (i.e., t_0), it was necessary to adjust the chopper to full open and then adjust the position of a light source to provide a peak output from the photodiode used for the start pulse. The chopper was designed to be open for less than one degree of rotation. During operation the leading edge of the start pulse from the chopper was double differentiated and input to the time-of-flight analyzer. This was done so that the start pulse to the time-of-flight analyzer would occur at the peak of the chopper start pulse. Various chopper speeds, time intervals per channel, and total number of channels were tried to obtain suitable spectrum definition and data accumulation rate. The values used were a chopper angular frequency of 100 radians per second, a time interval of four microseconds per channel and a total of 1024 channels.

Since 1024 channels were used for each spectrum with numerous corrections and conversions made to the data in each channel, it became apparent that a computer program would be necessary to reduce the chance of calculational error and the time for data analysis. A detailed explanation is given in Appendix A. The following were those quantities which were incorporated into the computer program:

1) A correction for the probability of detection vs. neutron energy for the BF_3 detector was used. Since the boron absorption cross-section curve is a straight line on a log plot, its equation of capture cross section vs. neutron energy is of the form $\sigma = bE^a$. The constants were evaluated and the equation was then used to correct for the probability of detection vs. neutron energy.
2) The aperture correction of the chopper (Appendix B) is a correction for the probability of a neutron with velocity v, traversing the chopper during the time the chopper window was open. The probability for a neutron with infinite velocity was 1.0 while the probability was zero for a neutron whose velocity was less than or equal to the cut-off velocity (v_{co}).
3) There was a correction for the change in energy per channel not being proportional to the "width" of the channel in time. This correction was built into the aperture correction as a function of time (Appendix B).
4) The velocity and energy corresponding to each channel was calculated. (i.e., 4 microsecond interval)
5) The data were normalized and the resultant curves plotted.

The time-of-flight analyzer does not have a memory associated with it and, therefore, uses the memory of another analyzer. In this case a TMC 1024 channel analyzer memory was used to accumulate the spectrum as a function of time (Figure 8). These data were then transferred onto punched paper tape and later converted to IBM data cards to be used by the computer.

The aperture correction that had been derived [12] was a function of neutron velocity derived from the flight time (i.e., flight length/neutron travel time). However, when this correction was applied to the time-of-flight data the resulting spectrum increased to infinite intensity at low neutron energies. Upon investigation it was realized that a new aperture correction would have to be derived as a function of flight time. The derivation of the aperture correction as a function of time is presented in Appendix B [11].

With the above corrections the neutron energy spectrum, which was obtained at a bulk reactor heavy water temperature of 320° K, exhibited a distribution similar to that of a Maxwell-Boltzmann distribution of $\emptyset(E)$ vs. E as shown in Figure 9. The peak occurred at approximately 0.045 electron volts which corresponds to a neutron temperature of 522° K. For comparison a Maxwell-Boltzmann distribution of $\emptyset(E)$ vs. E corresponding to a neutron temperature of 522° K is also plotted in Figure 9.

Figure 8. The uncalibrated observed distribution of counts per channel N(t) versus neutron flight time t, with N(t) the vertical axis and t the horizontal axis. The lower curve was observed for 10^3 counts in the peak channel with the upper curve having 10^4 counts in the peak channel

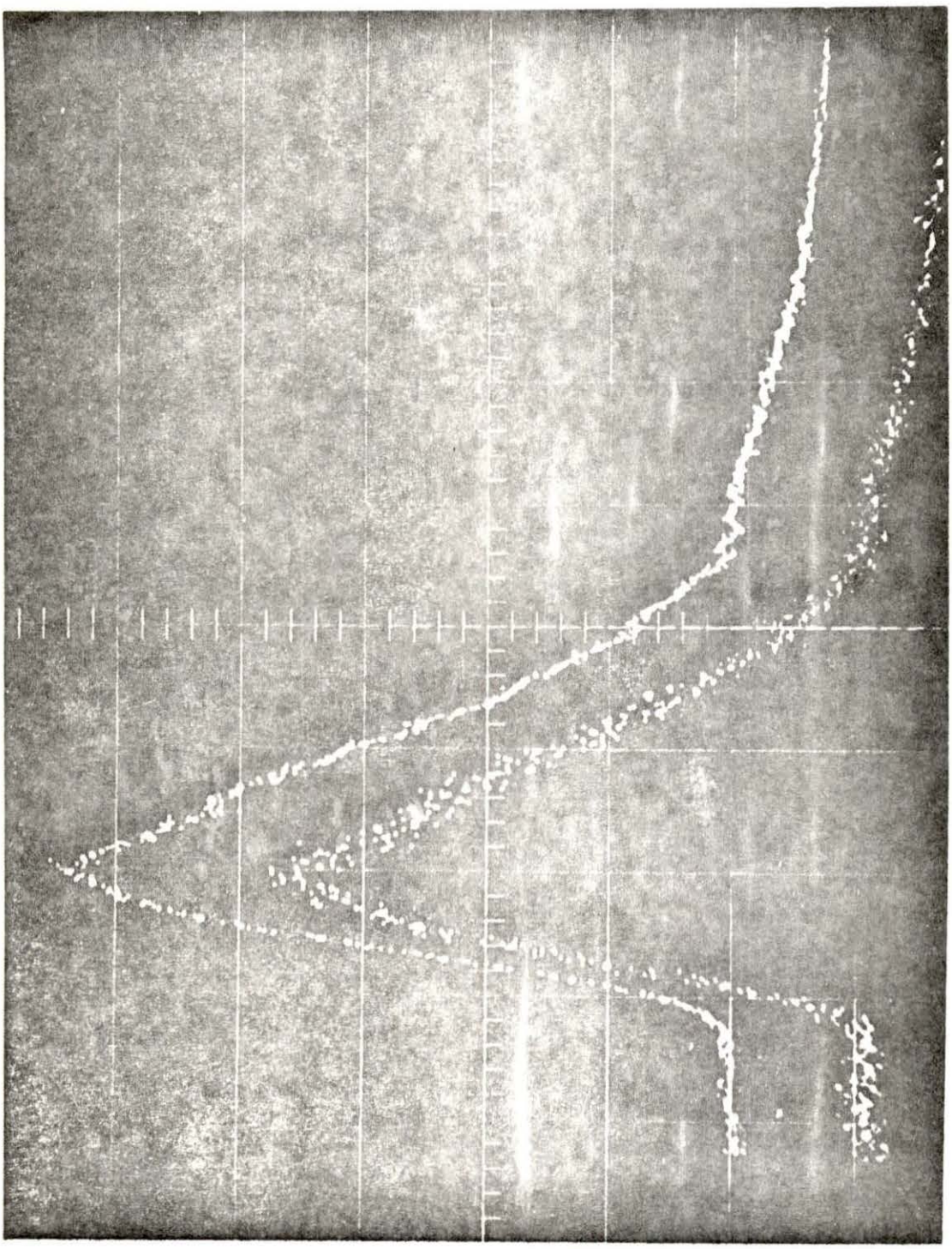

Figure 9. A typical unmodified neutron energy spectrum from the four inch beam port with a Maxwell-Boltzmann distribution

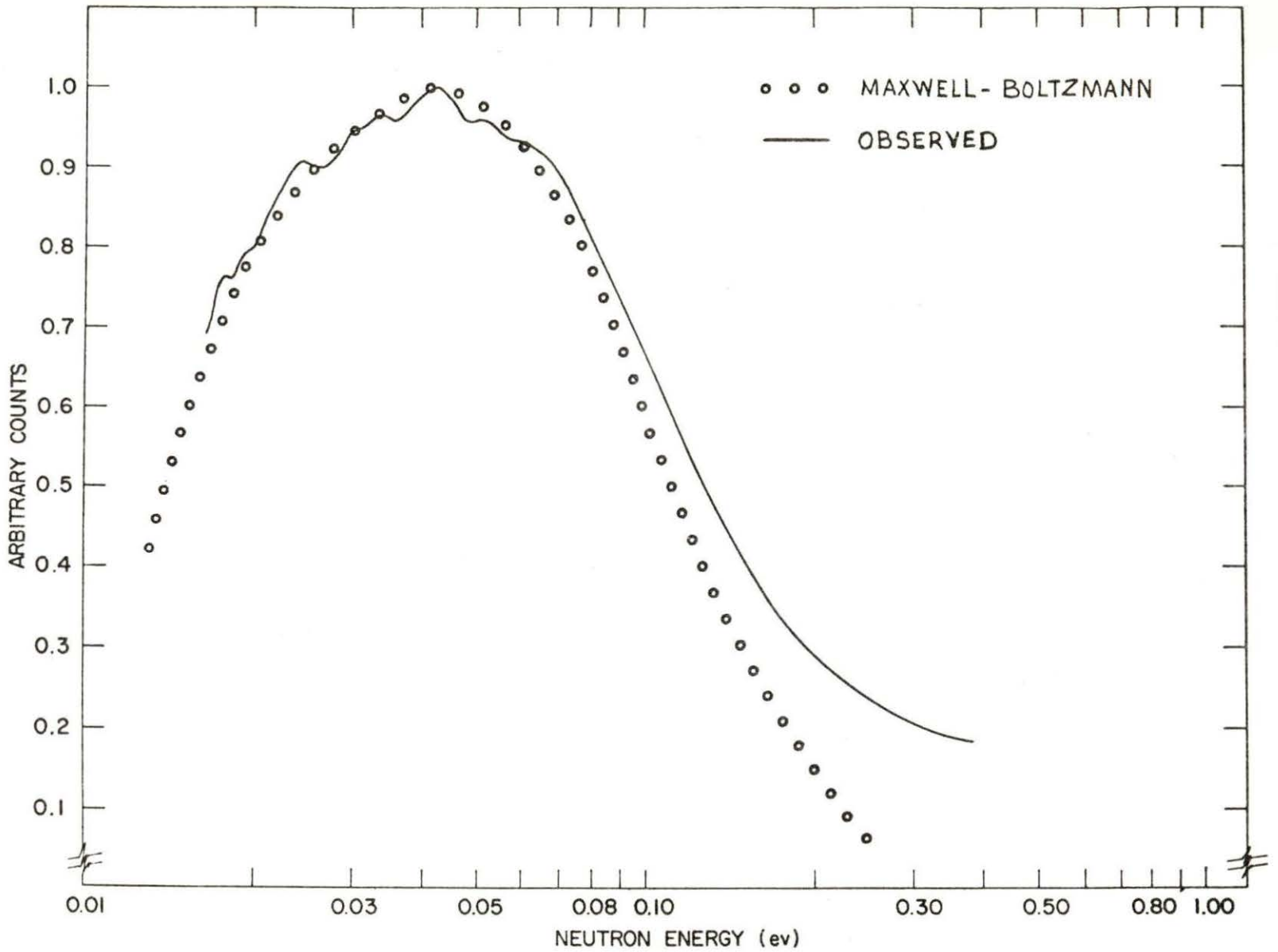
MAXWELL- BOLTZMANN
OBSERVED
ARBITRARY COUNTS
1.0
0.9
0.8
0.7
0.6
0.5
0.4
0.3
0.2
0.1
0.01
0.03
0.05
0.08
0.10
0.30
0.50
0.80
1.00
NEUTRON ENERGY (ev)

In order to check the experimental setup, equipment, procedure, computer program etc., an energy spectrum of the neutrons from the ALRR thermal column was obtained. Details of this spectrum are available and have been published [12]. The beam intensity was low and the background high, so that the statistical properties of the data obtained were not as desirable as that from the four-inch beam port. However, the most probable energy was found to occur at approximately 0.0425 electron volts which compares favorably with values found previously. The thermal column spectrum is shown in Figure 10 together with a Maxwell-Boltzmann distribution corresponding to a neutron temperature or 494° K.

While collecting data for a neutron energy spectrum, the experiment was run until there were at least 10,000 counts in one or more channels (i.e., one 4 microsecond interval). This value was chosen so that statistical variations would be small. The time required to accumulate the data was from four to fourteen hours, depending on the beam intensity.

Due to the amount of data accumulated and the sensitivity of the instrumentation, "fine structure" of the system could be observed in the energy spectrum. This "fine structure" was indicated by the irregularities in the spectrum, especially at lower energies (Figure 9). It was concluded that aluminum "windows" in the chopper (which were over three inches long) and other aluminum in the system was selectively scattering

Figure 10. The energy spectrum observed from the thermal column with the corresponding Maxwell-Boltzmann distribution

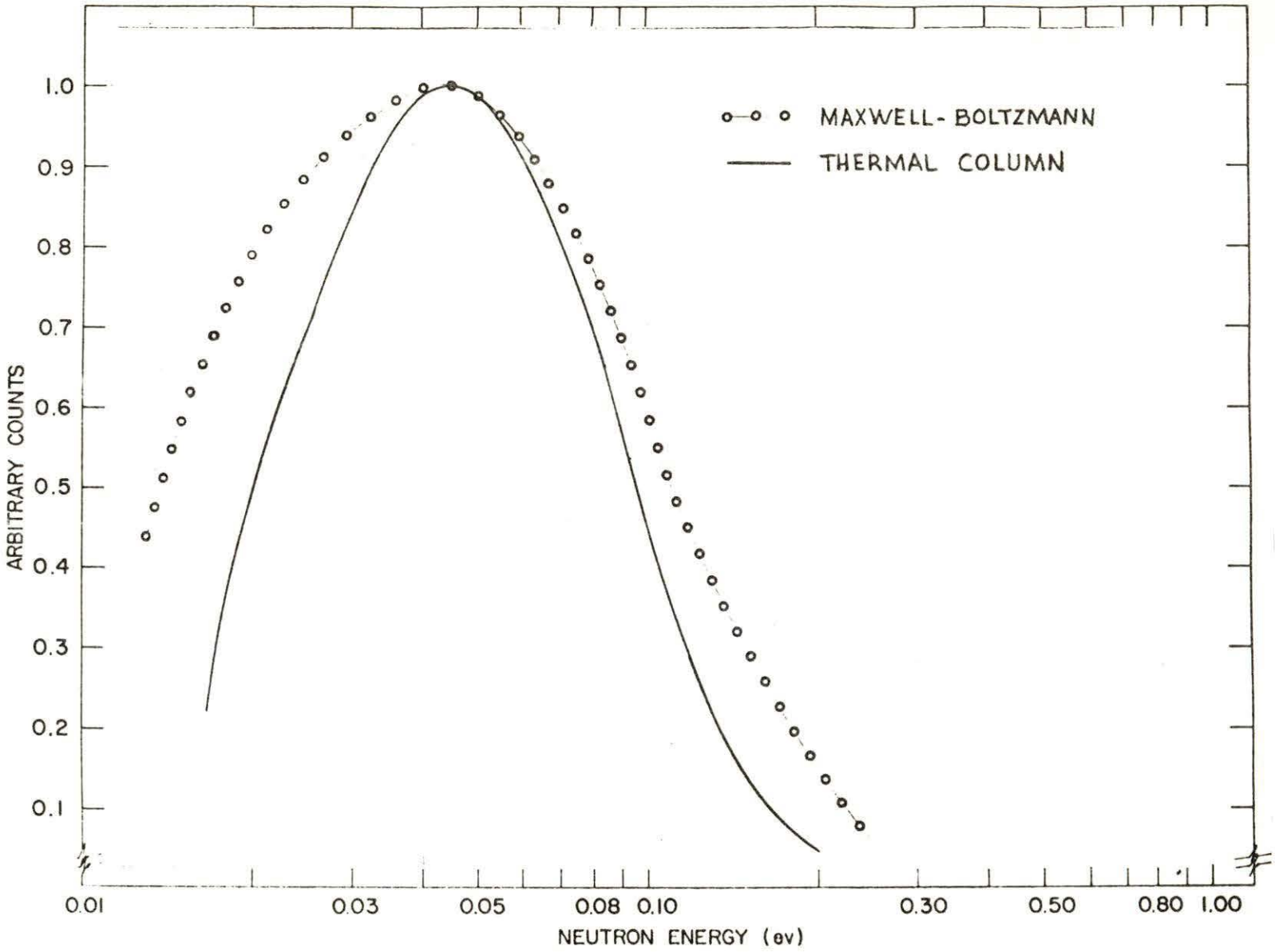
MAXWELL-BOLTZMANN
THERMAL COLUMN
ARBITRARY COUNTS
1.0
0.9
0.8
0.7
0.6
0.5
0.4
0.3
0.2
0.1
0.01
0.03
0.05
0.08
0.10
0.30
0.50
0.80
1.00
NEUTRON ENERGY (ev)

the neutrons [4]. The energies and relative intensities at which polycrystalline aluminum would scatter the neutrons were calculated and found to agree quite well with the observed irregularities (see Appendix D, and Figure 11).

Due to the selective scattering in aluminum the observed spectrum was not the complete spectrum. While the complete spectrum was not observed for the above reason, the effects on the spectrum by those variables tested were not changed. Also, scattering by the aluminum does not seriously hinder the observance of the effects.

The neutron scattering in the chopper provided an additional check on the system performance and showed that the system was giving the correct energy values.

As previously mentioned, the materials for which effects were observed were graphite, beryllium oxide, and beryllium metal. The tests were made by inserting cylinders or rods of the material which were one or two inches long into the thin walled aluminum material holding tube (Figure 4). This was accomplished by the following sequence of steps:

1) The reactor was shut down or sub-critical.
2) The fifty-two inch long collimator was removed.
3) A special tool for withdrawing the material-holding tube was inserted and used to withdraw the tube.
4) The next rod of material was then placed in the tube and the tube reinserted.

Figure 11. Neutron spectrum with calculated energies and relative magnitudes at which neutrons should be scattered by aluminum

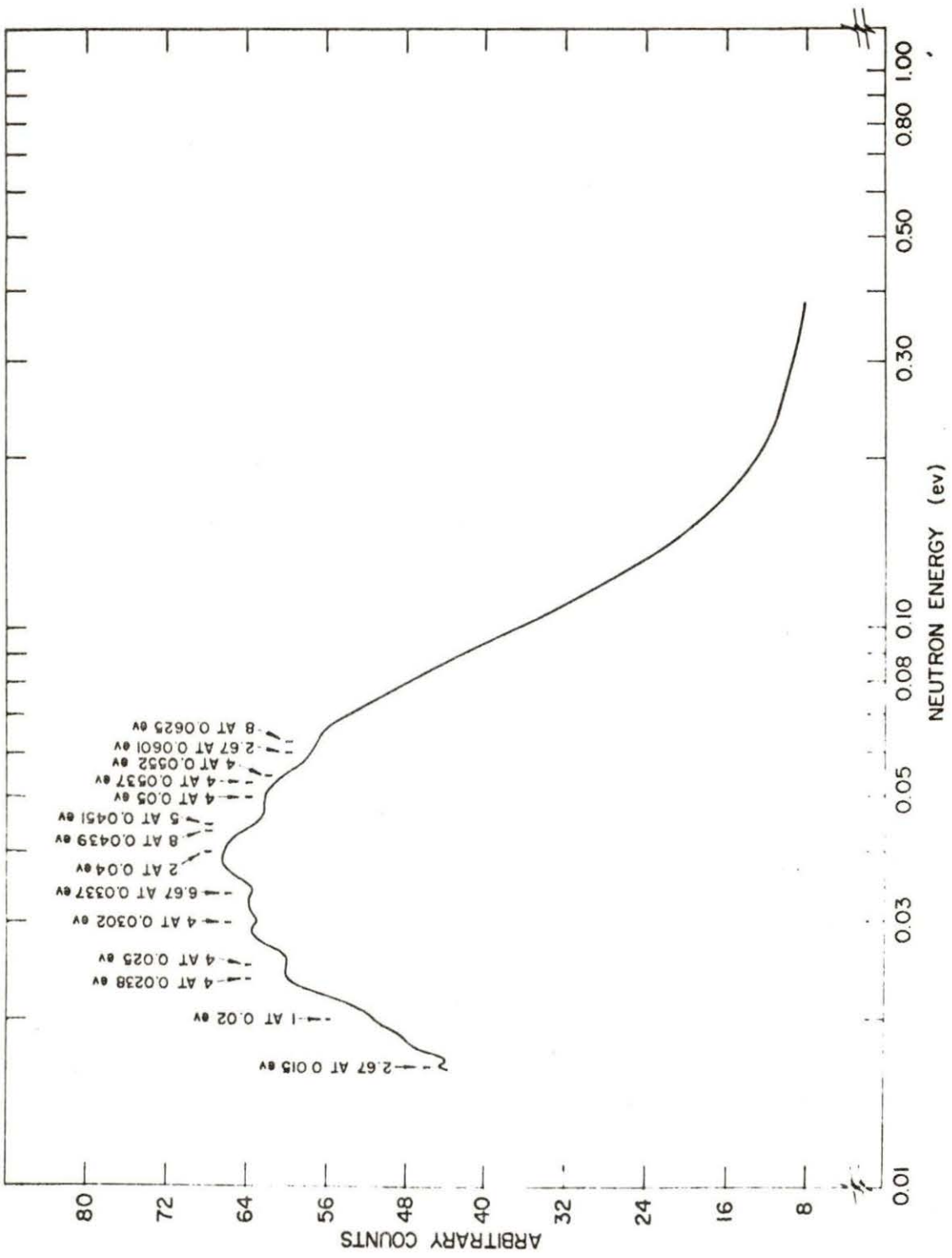
ARBITRARY COUNTS
80
72
64
56
48
40
32
24
16
8
NEUTRON ENERGY (ev)
0.01
0.03
0.05
0.08
0.10
0.30
0.50
0.80
1.00
2.67 AT 0.015 ev
1 AT 0.02 ev
4 AT 0.0238 ev
4 AT 0.025 ev
4 AT 0.0302 ev
6.67 AT 0.0337 ev
2 AT 0.04 ev
8 AT 0.0439 ev
5 AT 0.0451 ev
4 AT 0.05 ev
4 AT 0.0537 ev
4 AT 0.0552 ev
2.67 AT 0.0601 ev
8 AT 0.0625 ev

5) A long push rod was used to be sure the tube and material were at their full-in position.

6) The collimator was replaced.

After each rod of material was inserted and the reactor brought to its five-megawatt operating power, the following measurements were made:

1) The total neutron current was measured at the outer end of the collimator using a gold foil. This was accomplished using a foil holder which was placed in the collimator opening. The duration of activation was generally 45 minutes.

2) The epi-cadmium neutron current was obtained with the same procedure as above using cadmium covered gold foil. The thickness of cadmium used to surround the gold foil was 31 thousandths of an inch.

3) Data were then taken with the chopper and time of flight analyzer to determine the slow neutron energy spectrum.

The previous steps were repeated for up to ten inches total length of the materials tested.

The total neutron current from a reactor beam port was affected considerably by the axial neutron flux distribution in the core and core reflector region (Figures 12 and 13 [1]). If the reactor was operated at a fixed power, as was the case throughout this experiment, the position of the control rods

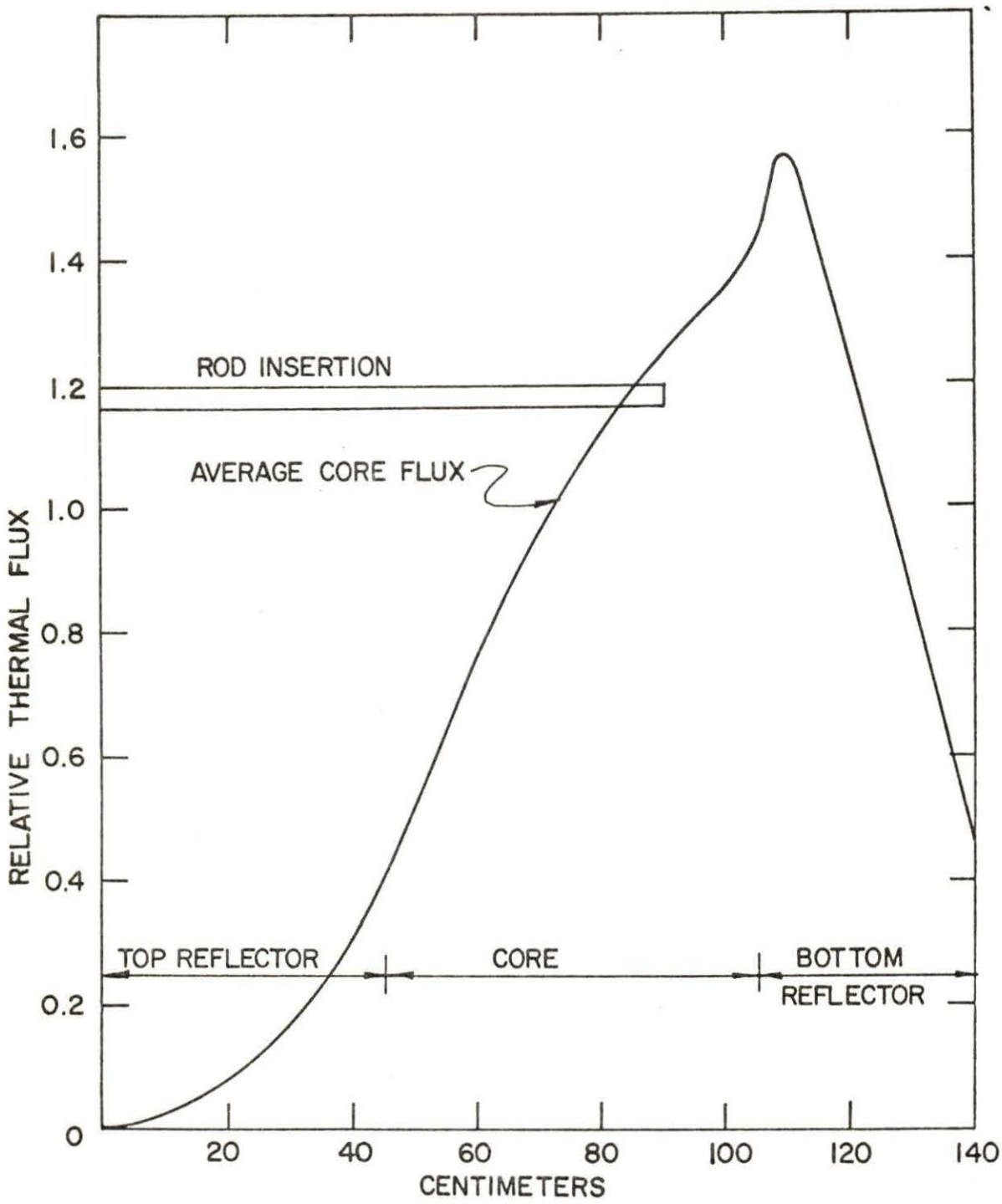

Figure 12. Axial neutron flux distribution with control rods inserted into 75% of the active core

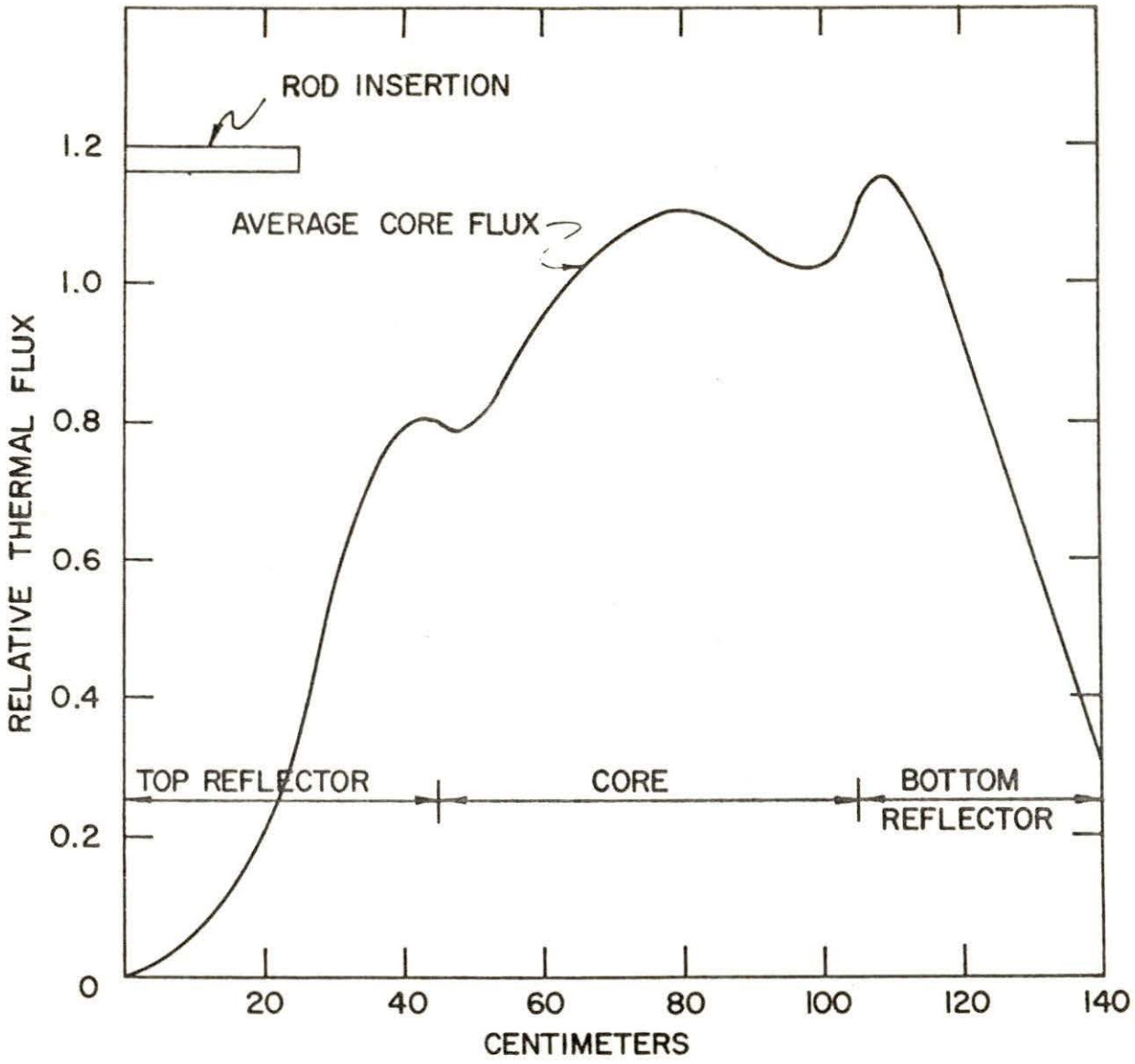

Figure 13. Axial neutron flux distribution with control rods fully withdrawn

was the primary variable for changing the axial flux distribution. Since the experiment was conducted over a period of more than one year, the position of the reactor control rods (hence the axial flux distribution) varied between 39% and 97% withdrawn. The JRR-II[1], design manual [1] gives axial neutron flux distributions as a function of control rod position. Figures 12 and 13 show two of the distributions. It was hoped that a correction for total beam port current as a function of control rod position (for a fixed reactor power) could be obtained from these curves. However, it was noted that these curves were obtained for the cold clean critical condition using two group diffusion theory. After checking these against experimental data, a decision was made to obtain experimental data relating control rod bank withdrawal vs. total neutron beam port current. The resulting data are plotted in Figure 14. Figure 14 illustrates that the total beam port current could vary by more than 20% throughout the life of the reactor core (fuel) with the power fixed. The observed reproducibility of the data points for this correction curve was $\pm$5%.

---

[1]JRR-II is the Japanese Research Reactor II which is identical in most respects with the ALLR.

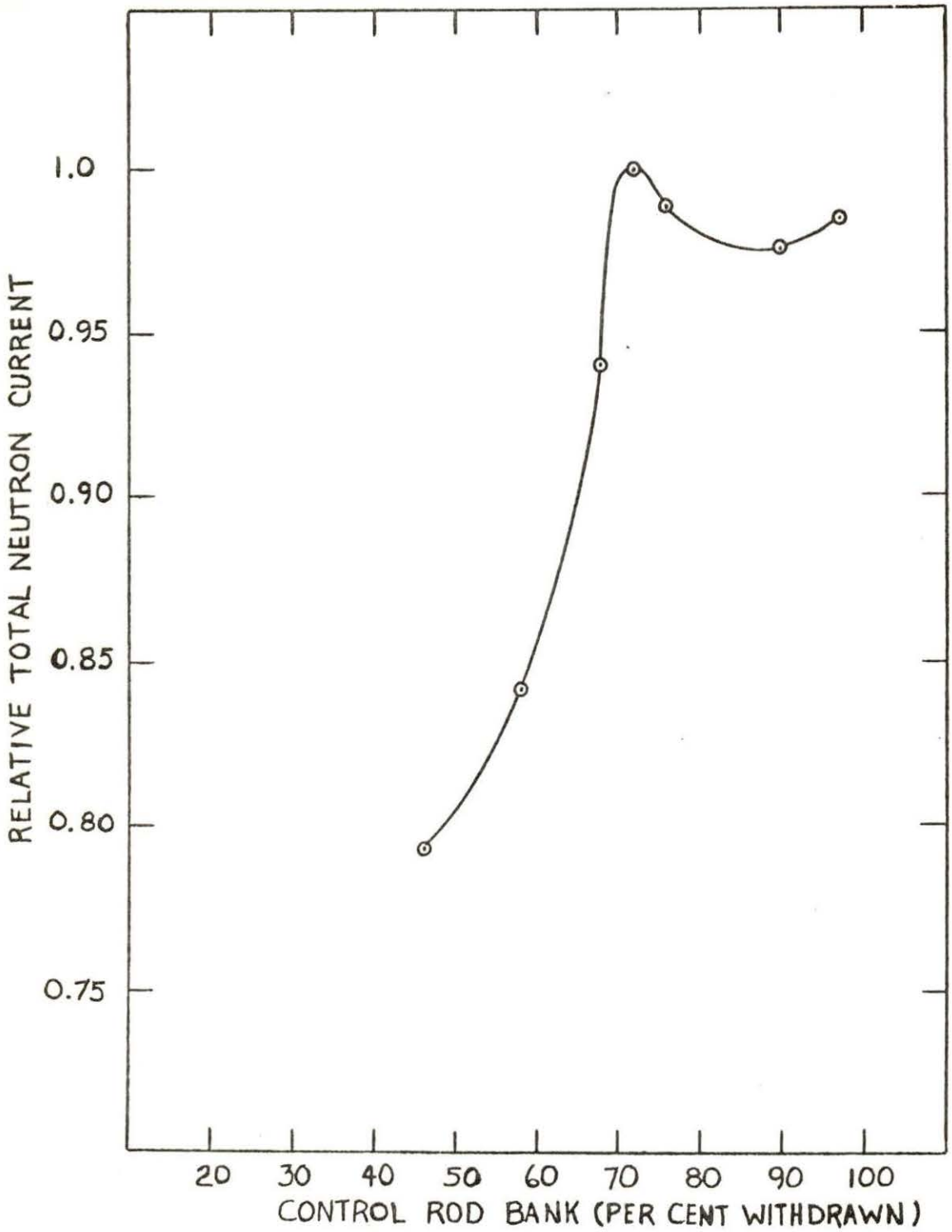

Figure 14. Total neutron beam port current versus control rod bank position at 5 MWth for the H-4 beam port at the ALRR

RESULTS

The data obtained as counts per channel were analyzed using the DATARE computer program (see Appendix A). The resulting slow neutron energy spectra were plotted by the "SIMPLOTTER" which is an auxiliary output system of the Iowa State University IBM-360 computer. Experimental data points were not indicated since they were so close together they would tend to smear the curves.

A typical slow neutron energy spectrum from the four-inch beam port is given in Figure 9. The energy range displayed is from 0.0164 electron volts to the cadmium cutoff at approximately 0.4 electron volts. The actual spectrum was expected to approximate a Maxwellian distribution; however, the aluminum in the system caused selective scattering of the incident beam. The spectrum in Figure 9 corresponds to the direct beam from the beam port which had not been altered by material in the beam tube. The reactor was operating at five megawatts thermal power with a bulk moderator temperature of 125°F and an average control rod bank position of 85% withdrawn.

The addition of material into the material-holding tube required that the reactor be shut down. Since no reactor shutdowns were scheduled for these experiments, waiting for shutdowns introduced time delays between slow neutron energy spectrum measurements. This operational requirement along with the assumption that the unmodified spectrum would not

change to any great extent from experiment to experiment were the reasons for obtaining only three unmodified energy spectra.

The initial, or reference, slow neutron energy spectrum with an unmodified beam was obtained with the reactor control rod bank at 39% withdrawn and a reactor bulk temperature of 114°F. The only other unmodified spectra observed were for control rod bank positions and reactor bulk temperatures of 79% at 123°F and 85% at 125°F. The unmodified spectra for minimum and maximum observed control rod positions are given for comparison in Figure 15. The spectra were normalized to equal area under each cure. While some error was associated with these two spectra (see Appendix C), significant spectral differences are evident. The difference in bulk D_2O temperature for these spectra was only 6.1° K which corresponds to an energy change $E = kT = (8.6167 \times 10^{-5}$ ev./°K) (6.1°K) = 5.25×10^{-4} eV.

Table I defines the conditions and gives quantitative differences between the two spectra. The spectra were arbitrarily broken into four regions for comparison. The value of temperature T in kT, used to define region break points is 503° K which corresponds to the most probable neutron energy of the reference spectra observed at an average rod bank of 39% withdrawn.

Typical slow neutron energy spectra are given in Figure 16 for an unmodified beam and with additions of graphite as a

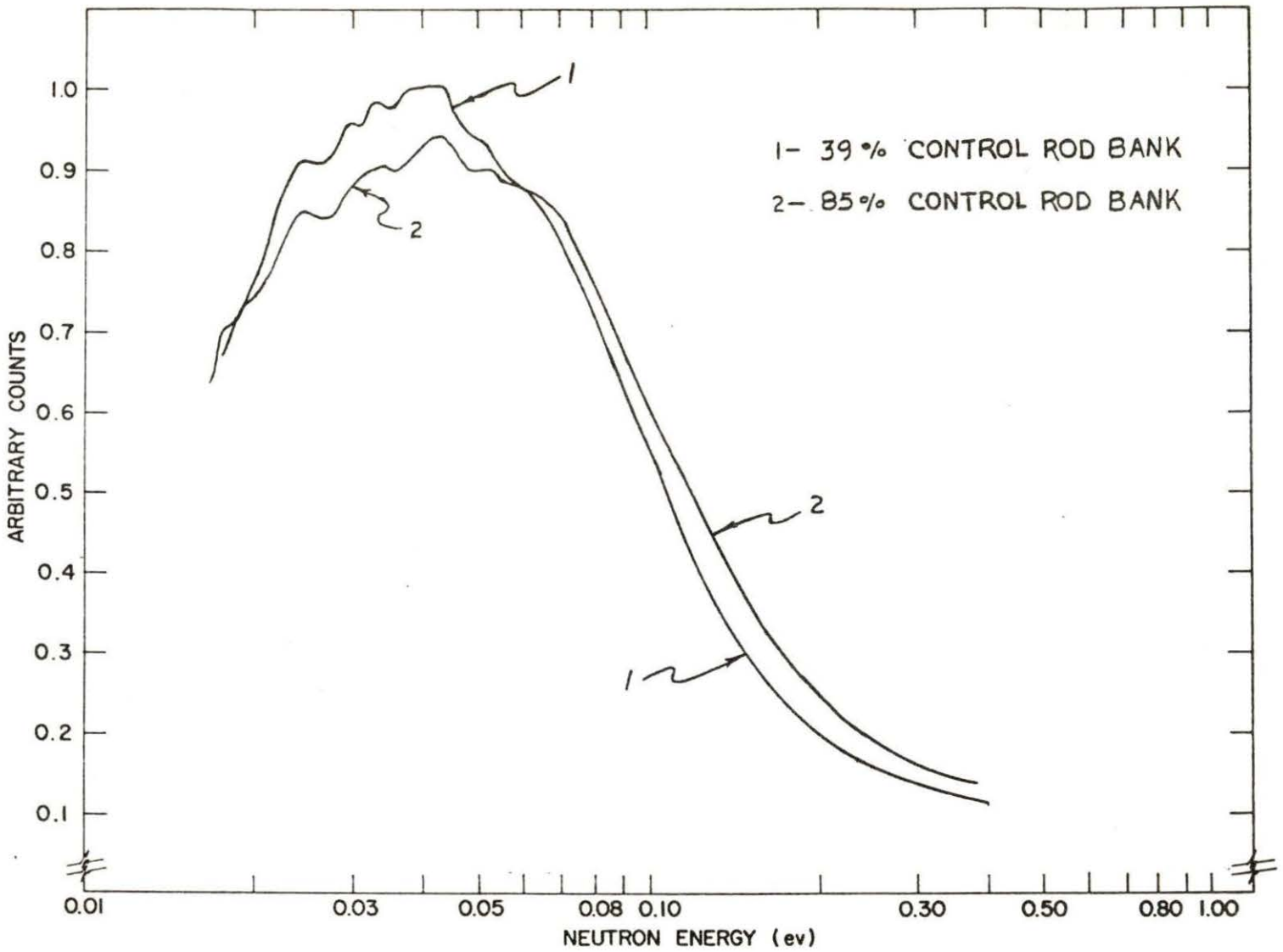

Figure 15. The observed spectral shift between control rod bank positions of 39% and 85% withdrawn

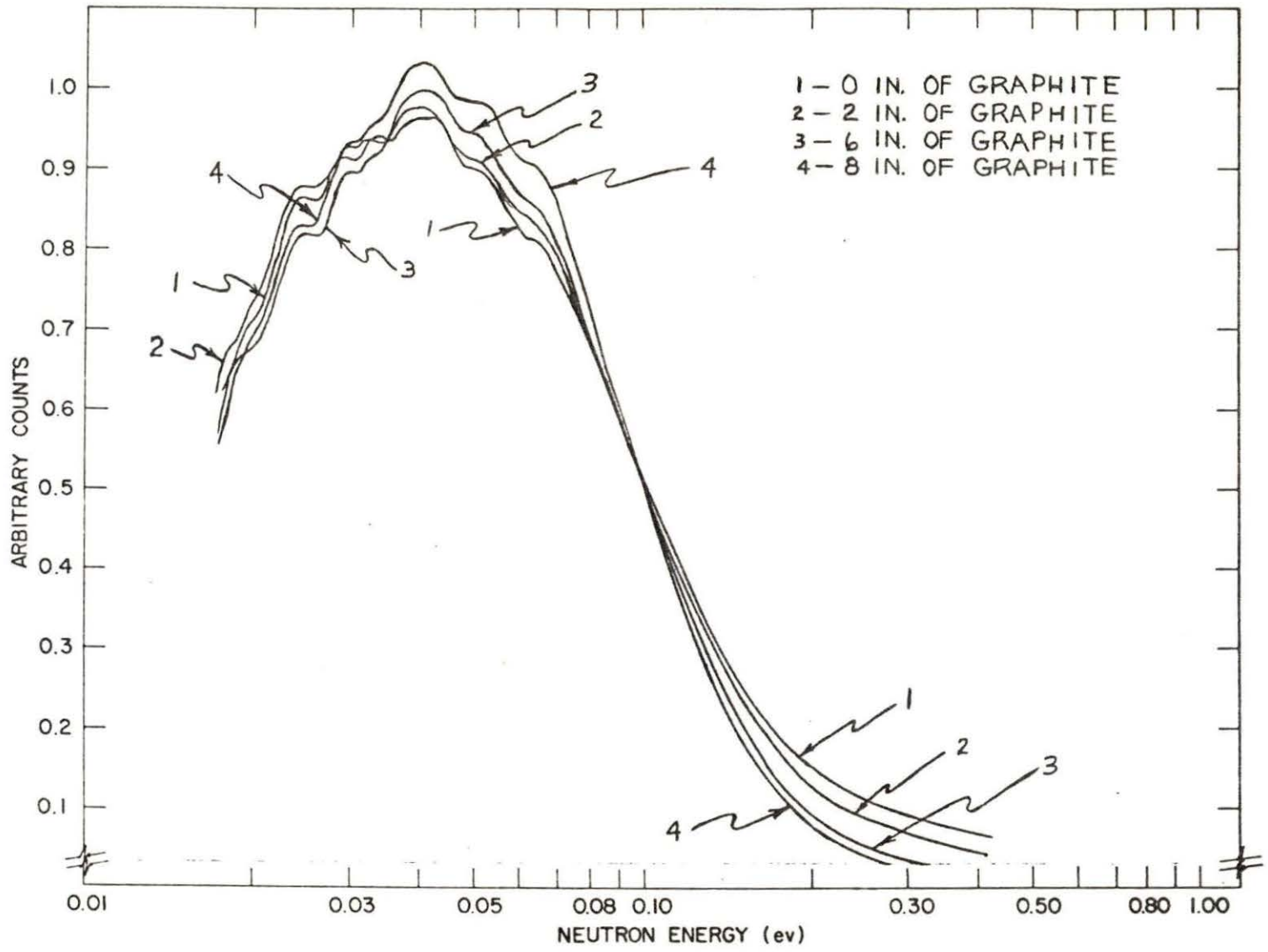

Figure 16. Spectrum variations with additions of graphite

Table I. Conditions for spectral shift data and differences observed

Avg. cont. rod bank (% with.)	Bulk D_2O temp. (°F)	Avg. neut. energy (eV)	Avg. neut. velocity (M/sec)	% change for 0.0164eV to kT	% change for kT to 2kT	% change for 2kT to 5kT	% change for 5 kT to 0.40 eV
39	114	0.05436	3000	--	--	--	--
85	125	0.05534	3023	-4.5	+2.5	+15.8	+6.6

scattering and moderating medium. The spectra have been normalized such that they exhibit equal area. Conditions under which the spectra were observed are given in Table II. The effect of increased control rod withdrawal position was to increase the population of higher energy neutrons. However, no correction has been made here to compensate for this effect.

Table II. Conditions for the spectra of Figure 16

Curve #	Date	Reactor power	Average reactor cont. rod bank	Bulk D_2O temp. (°F)	Length of material in beam tube (in.)
1	1/31/68	5MWth	39%	114	0.0
2	2/17/68	5MWth	41%	113	2.0
3	3/2/68	5MWth	46%	110	6.0
4	3/9/68	5MWth	48%	111	8.0

In each case the material was against the inner end of the beam tube as shown in Figure 4.

Table III gives a complete list of those conditions tested for graphite. Again the energy break points are referenced to 503°K. Percent deviations from the reference unmodified spectrum are also tabulated. Average neutron energy and velocity exhibit a general decreasing trend with increased graphite, as would be expected. For the first region (0.0164 eV to kT), no significant variation in neutron population is observed with increasing amounts of graphite. The range in energy from kT to 2kT exhibits a trend toward increasing

Table III. Results of spectrum modification with graphite

Length of graphite in beam tube (in.)	0.0	1.0	2.0	4.0	6.0	8.0
Date	1/31/68	2/16/68	2/17/68	2/38/68	3/2/68	3/9/68
Bulk D_2O temp. (°F)	114	109	113	112	110	111
Avg. cont. rod bank (%)	39	41	41	45	46	48
Avg. neut. energy (eV.)	0.05436	0.05150	0.05111	0.05196	0.05057	0.04904
Avg. neut. velocity (m/sec)	3000	2934	2922	2956	2930	2896
% dev. from ref. for 0.0614 eV to kT	--	-1.7	-1.1	-2.2	-1.9	-1.0
% dev. from ref. for kT to 2kT	--	+4.2	+3.4	+6.6	+10.0	+11.5
% dev. from ref. for 2kT to 5kT	--	+2.3	+1.2	+1.6	-4.6	-10.8
% dev. from ref. for 5kT to 0.4 eV	--	-15.0	-16.0	-27.3	-40.7	-50.8

neutron population with increased graphite, however, some fluctuations in the data are observed. Appendix C is an error analysis which illustrates possible errors which could account for these variations. In the region of 2kT to 5kT an increase in neutron population is exhibited for small increases in graphite length, however, a decrease is then observed for large increases in graphite length. The reasons for this behavior are not completely understood. The high energy region exhibits a strong trend (6.35%/in.) toward decreasing neutron population with increasing amounts of graphite.

The temperature of a large block of graphite at the inner end of a beam tube has been measured at the ALRR. The graphite block reached a temperature of 500°F with the reactor at its full rated power of 5 MWth. Therefore, under the conditions of this experiment the graphite is expected to have been in the range of 400 to 700°F.

Figure 2 illustrates a strong radial gradient in the neutron flux. In order to observe the effect of this gradient, the total neutron current was measured with a gold foil for the case of one inch of graphite full in and three inches withdrawn from full in. With all other experimental conditions constant, the change was measured to be a 22% decrease in the total neutron current.

Typical changes in the slow neutron energy spectrum due to additions of beryllium oxide as the scattering and moder-

ating medium are given in Figure 17. The spectra have been normalized such that they have equal area under each curve. Conditions under which the spectra were observed are given in Table IV. Here again, no correction has been made for the effect of increased population of higher energy neutrons with greater control rod withdrawal.

Table IV. Conditions for the spectra of Figure 17

Curve #	Date	Reactor power	Average reactor control rod bank	Bulk D_2O temp. (°F)	Length of material in beam tube (in.)
1	1/31/68	5MWth	39%	114	0.0
2	5/10/68	5MWth	62%	112	3.12
3	5/20/68	5MWth	64%	110	6.25
4	5/28/68	5MWth	69%	111	10.14

In each case the material was against the inner end of the beam tube. Based upon the measured temperature of graphite and the fact that the oxide will conduct heat less readily it is expected that the BeO temperature was in the range of 500° to 800°F. The BeO used was high purity (99.5%) with a density of 2.85 grams per cubic centimeter.

Those conditions which were tested for beryllium oxide are given in Table V. The energy break points are increments of kT which is referenced to 503° K. Percent deviations from the reference unmodified spectrum are also tabulated for the four regions chosen. Average neutron energy and velocity do

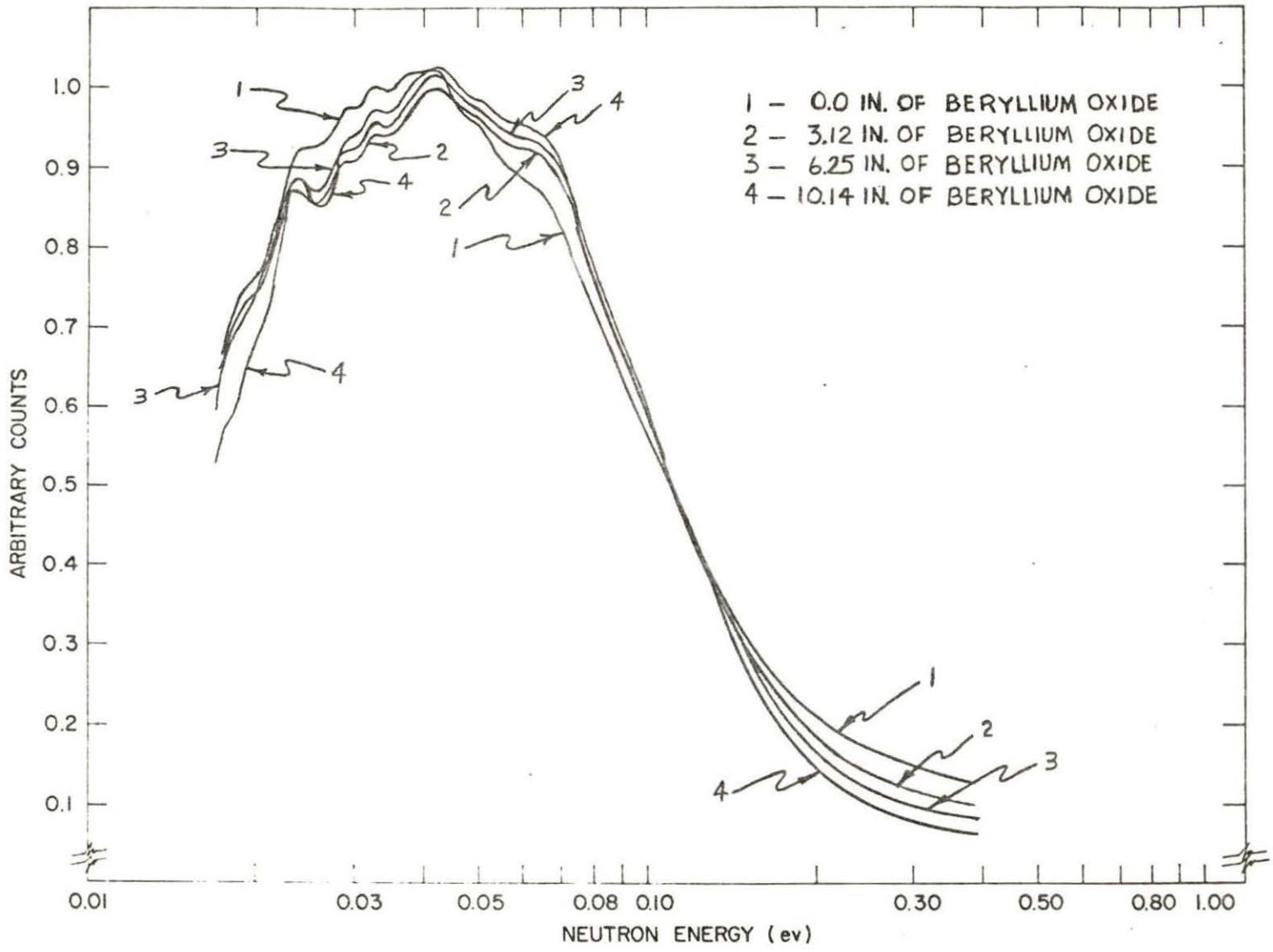

Figure 17. Spectrum variations with additions of beryllium oxide

Table V. Results of spectrum modification with beryllium oxide

Length of beryllium oxide in beam tube (in.)	0.0	0.781	1.562	3.12	4.686	6.25	7.810	10.14
Date	1/31/68	5/3/68	5/6/68	5/10/68	5/14/68	5/20/68	5/23/68	5/28/68
Bulk D_2O temp. (°F)	114	110	112	112	114	110	115	111
Avg. cont. rod bank (%)	39	58	60	62	62	64	67	69
Avg. neut. energy (eV)	0.05436	0.05304	0.05290	0.05301	0.05244	0.05153	0.05209	0.05083
Avg. neut. velocity (m/sec)	3000	2971	2973	2985	2976	2946	2980	2954
% dev. from ref. for 0.0164 to kT	--	-1.9	-2.3	-2.4	-2.6	+0.8	-4.2	-3.4
% dev. from ref. for kT to 2kT	--	+2.9	+5.1	+7.1	+8.4	+3.3	+12.6	+13.8
% dev. from ref. for 2kT to 5kT	--	+4.8	+3.9	+13.0	+14.6	-3.9	+2.6	-2.1
% dev. from ref. for 5kT to 0.4 eV	--	-8.0	-17.2	-25.9	-35.3	-36.3	-48.3	-59.2

not exhibit any significant trend with increased amounts of beryllium oxide. For the first region (0.016 eV to kT) a slight decrease in neutron population is observed with increasing amounts of BeO. The trend here is weak (0.5%/in.) with significant fluctuations in the data (see Appendix C). This decrease in intensity is due to the higher temperature and increased macroscopic absorption cross section of the BeO compared to that of the heavy water. The range of energy from kT to 2kT exhibits a trend toward increasing neutron population with increased BeO. The trend is more pronounced than in the same range for graphite.

A trend similar to that of graphite is observed for the range of 2kT to 5kT. The reason(s) for the trend of increasing then decreasing neutron population with increasing beryllium oxide length, has not been determined. However, it is possible that due to the steep radial flux gradient a point is reached where few neutrons in this energy range are scattered into the beam with increased material. Thus, the increased material only serves to moderate those neutrons in the beam.

The high energy range again exhibits a strong trend (5.84%/in.) toward decreasing neutron population with increasing amounts of BeO. This trend is not as pronounced as that observed for graphite (6.35%/in.).

Typical changes in the slow neutron energy spectrum due to additions of beryllium metal as the scattering and moderating medium are given in Figure 18. The spectra have been

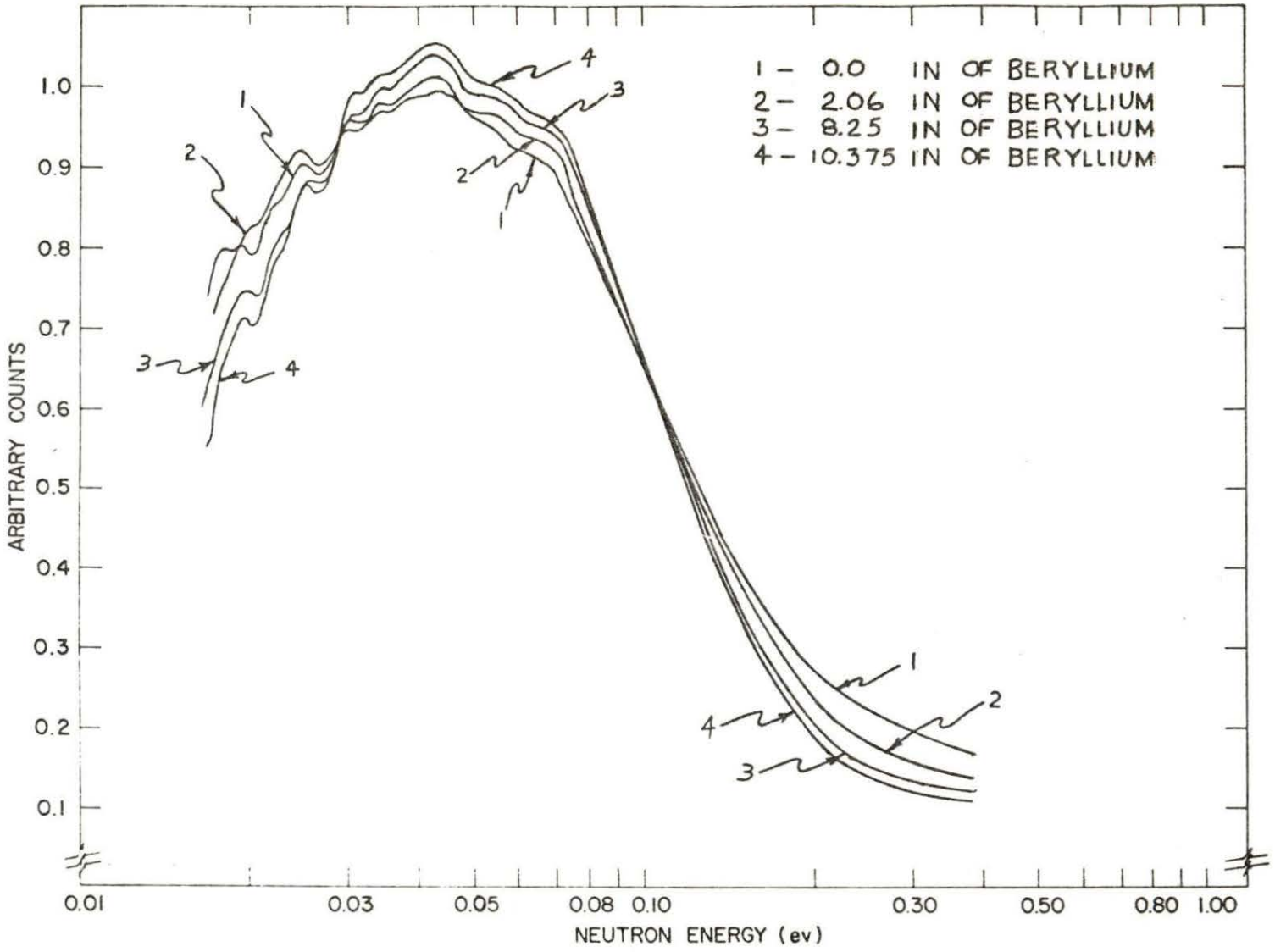

Figure 18. Spectrum variations with additions of beryllium metal

normalized so that they encompass equal area. Conditions for the spectra illustrated in Figure 18 are given in Table VI. No correction has been made for spectral shift with control rod bank variations.

Table VI. Conditions for typical observed spectra with Be metal

Curve #	Date	Reactor power	Reactor control rod bank	Bulk D_2O temp. (°F)	Length of material in beam tube (in.)
1	7/17/68	5MWth	79%	123	0.0
2	6/5/68	5MWth	73%	119	2.06
3	7/3/68	5MWth	80%	115	8.25
4	7/5/68	5MWth	82%	118	10.375

An estimate of the beryllium temperature, which is above ambient, due to radiation heating and the energy liberated by the gamma-neutron reaction in beryllium, is in the range of 450° to 800°F. This estimate is based on the measured temperature of graphite and the fact that beryllium metal will conduct heat readily. Gamma flux in the area of the materials is estimated to be 10^8 R/hr. The beryllium metal used for this phase of the experiment was 98.4 weight percent Be metal with 2 weight percent BeO and trace amounts of other impurities which have very low neutron capture cross sections. Density of the Be metal used was 1.845 gms/cm^3.

Table VII tabulates the conditions which were tested for Be metal. The arbitrary energy regions are the same as those

Table VII. Results of spectrum modification with beryllium metal

Length of beryllium in beam tube(in.)	0.0	1.031	2.063	4.125	6.188	8.250	10.375
Date	7/17/68	6/3/68	6/5/68	6/7/68	7/2/68	7/3/68	7/5/68
Bulk D_2O temp.(°F)	123	118	119	120	111	115	118
Avg. cont. rod bank (%)	79	72	73	73	76	80	82
Avg. neut. energy (eV)	0.05406	0.05420	0.05294	0.05163	0.05031	0.05043	0.04957
Avg. neut. velocity (m/sec)	2989	3004	2977	2998	2929	2935	2906
% dev. from ref. for 0.0164 to kT	--	-1.3	+0.4	-2.3	-0.7	-2.3	-0.1
% dev. from ref. for kT to 2kT	--	+3.8	+3.6	+8.2	+10.1	+12.0	+8.3
% dev. from ref. for 2kT to 5kT	--	+0.1	-4.7	-1.2	-8.0	-4.9	-6.8
% dev. from ref. for 5kT to 0.4 eV	--	-11.6	-22.8	-30.0	-50.5	-51.9	-53.0

used previously in this section. The reference unmodified spectrum was obtained for a control rod bank position of 79% withdrawn. Average neutron energy and velocity do not exhibit any significant trend with increased amounts of Be metal. For the lowest arbitrary energy region (0.0164 eV to kT) the previously observed trend of a slight decrease in neutron population with increasing material continues. The decrease in this low energy region was again due to the higher temperature and increased macroscopic absorption cross section of the Be metal compared with that of the heavy water. The range of energy from kT to 2kT yields a similar trend to that of graphite and beryllium oxide. The degree of increase in neutron population with increased material is approximately constant in this energy region for those materials tested. In the range of 2kT to 5kT a general decrease in neutron abundance with increasing amounts of beryllium metal is noted. This indicates a greater degree of neutron moderation in this energy range for Be metal than either graphite or beryllium oxide. For the energy range of 5kT to 0.40 eV a rapid decrease in neutron population with increasing length of Be metal is exhibited. The trend here is not as pronounced (5.10%/in.) as either graphite (6.35%/in.) or BeO (5.84%/in.).

In addition to the spectral change with reactor control rod position, there were other possible errors associated with the experimental apparatus and methods used. A computer

program was developed and used to determine the effect on the spectra of these variables. A discussion of the error analysis methods and results are given in Appendix C.

The curves of relative total neutron current versus length of material in the beam tube for the three materials tested are given in Figure 19. These curves have been corrected for the effect of control rod position (change in axial flux distribution) on the total neutron current. No correction has been made for the spectral shift (as illustrated in Figure 15) with control rod position. The spectral shift would cause some small error, since the gold foils used to measure the total neutron current have a cross-section proportional to 1/v.

Figure 20 indicates the change in cadmium-ratio with increasing lengths of material in the beam tube. The effect of the observed spectral shift with control rod position would have caused more error in the cadmium-ratio measurement than total neutron current measurement, due to the resonance absorption of gold above approximately 2 electron volts.

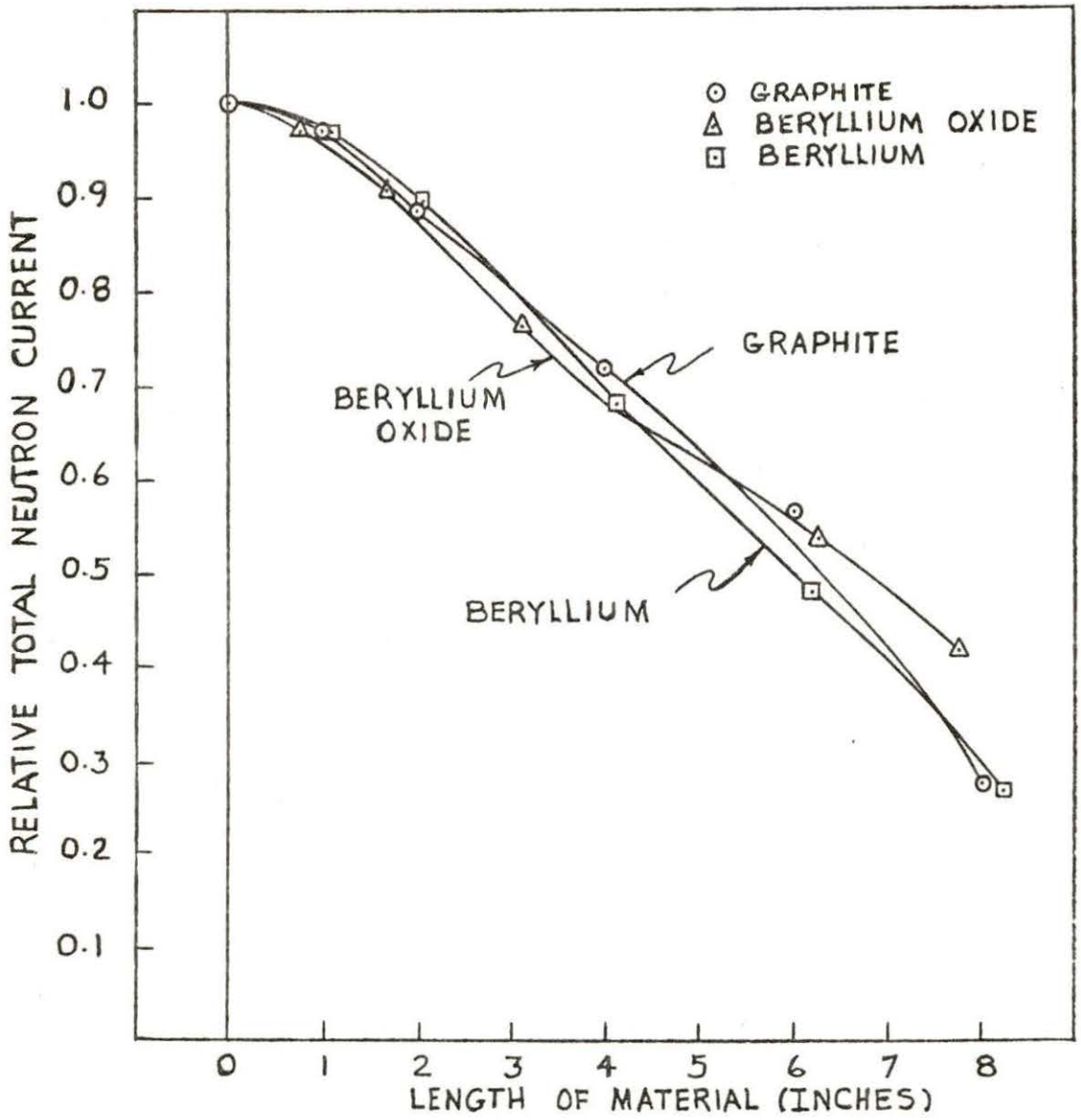

Figure 19. Relative total neutron current variations with additions of material

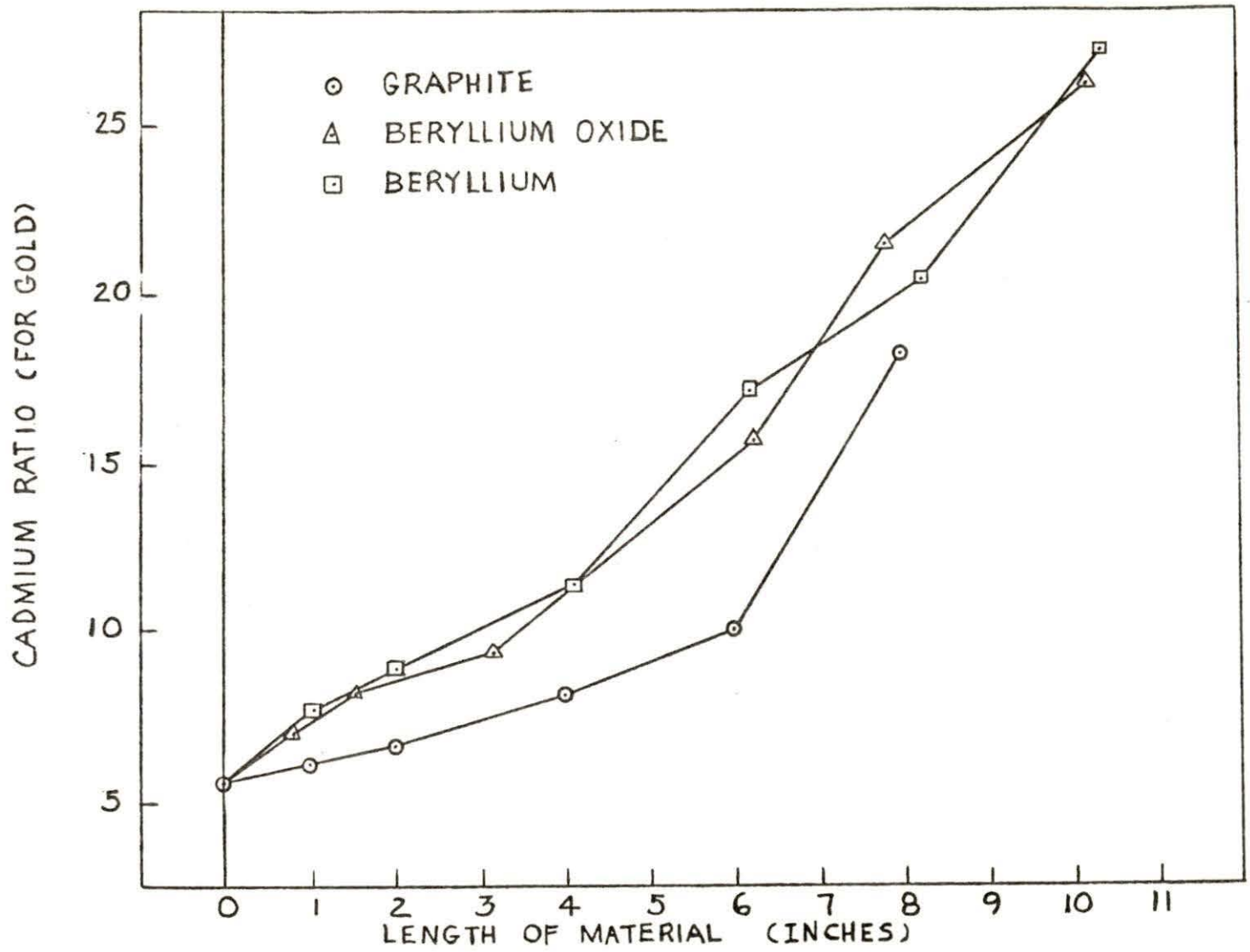

Figure 20. Variation of cadmium ratio with additions of material

CONCLUSIONS

It was suggested that an increase in total neutron current might be observed with the addition of a scattering material at the inner end of the beam tube. An increase was not revealed by the results of this experiment. However, the inner end of the beam tube was away from the edge of the core and beyond the thermal flux peak illustrated in Figure 2. Also, materials with much higher macroscopic scattering cross sections than heavy water were not tested. Therefore, the expectation of increased neutron current under appropriate conditions was not conclusively eliminated. The data of Figure 19 do not exhibit an exponential decrease in neutron current that might be expected if neutrons traveling parallel to the beam tube were the only contributing component. The decrease of 22% in total neutron current observed when a one-inch piece of graphite was pulled back three inches from its full-in position, further illustrates that a significant amount of "non-parallel" components of neutron flux can be incorporated into the exiting beam. Since the component of the flux which is parallel to the beam tube has a larger fast neutron component than the non-parallel flux, it would be advantageous to increase the initially non-parallel and decrease the parallel component of the neutron flux.

From the results of this experiment, the following conclusions were determined :

1. For best results the scattering material used should be as close to the inner end of the beam tube as possible;

2. There is a significant spectral shift observed at a beam port as the axial flux distribution changes (i.e., core burns out);

3. The total neutron current from a beam port may vary considerably (on the order of 25%) through the life of the reactor core for a fixed power level;

4. Additions of those scattering materials tested produced a relative increase in neutron population for the kT to 2kT region.

The information presented in this thesis is not intended as an optimized set of data. Rather it is intended to be used as a guide. For instance, an experimenter who is performing neutron diffraction studies usually is interested in neutrons with a wave length of one Ångstrom (i.e., 0.0825 ev). Thus, he may want to use beryllium oxide heated by radiation, since of the materials tested beryllium oxide exhibited the greatest relative intensity increase of the neutrons with energies near 0.08 electron volts. However, it should also be noted that the addition of material into the beam tube decreases the total neutron current. Therefore, if the experimenter can use the modified beam and shield externally for the unwanted radiations, it may be to his advantage. These data would then be only a part of the information needed to make the decision of how to enhance the neutron beam.

When selecting a material to be used in the manner described, consideration of properties other than nuclear

should be included. When materials are placed near a reactor core, they will be affected by the radiations (i.e., during this experiment the materials were subjected to a thermal neutron flux of greater than 5 x 10^{13} n/cm^2-sec. and a gamma dose rate on the order of 10^8 R/hr). The radiation can cause chemical composition changes, swelling, decreased tensile strength, high temperature buildup, etc. When designing a facility it is important to consider dimensional stability and chemical change (i.e., if a large block of beryllium had been used in this experiment it would have melted). The materials used in this experiment showed no signs of increased brittleness, dimension change or discoloration. However, the longest exposure was only four months.

The results of this experiment indicate that greater accuracy could have been obtained if the experiment had been performed over a much shorter time. The shorter time would render unnecessary the corrections for total neutron current and spectral shift versus control rod bank position with respect to the beam port.

SUGGESTIONS FOR FUTURE WORK

During this investigation several areas of interest for future study have become apparent. The following list indicates the possible study areas together with reasons for their usefulness.

1.) The effects of using larger diameter samples (i.e., 3, 4, or 5 inches in diameter) would be informative. Larger diameter samples would concentrate more scattering material in the higher flux region. The result may be to scatter more neutrons into the beam and increase the cadmium ratio for the same thickness or length.

2.) Experiments could be performed which may determine the actual location of the thermal flux peak as illustrated in Figure 2. If the location of this peak could be obtained, one may concentrate scattering material in this region and determine whether an increase in thermal flux can be achieved.

3.) A series of spectrum measurements could be performed at a beam port to define the variations and degree of the spectral shift with control position. The spectral variations during the course of an experiment could be very useful to an experimenter.

LITERATURE CITED

1. American Machine and Foundry Company, Engineering Design for Japan Research Reactor II, Vol. 1, Greenwich, Conn., Author (ca. 1959).

2. T. O. Brun and S. K. Sinha, "A Preliminary Report on the Triple-Axis Spectrometer at the Ames Laboratory Reactor," Unpublished, (ca. 1966).

3. J. B. Bullock, E. A. Daniels and J. S. King, Trans. Am. Nucl. Soc., 8 302 (May 1965).

4. P. A. Egelstaff, Thermal Neutron Scattering, pp. 206-208, Academic Press Inc., New York, New York (1965).

5. E. Frank, Electrical Measurement Analysis, pp. 167-169, McGraw Hill, New York, New York (1959).

6. C. G. James and D. A. Meneley, J. Brit. Nuclear Energy Soc., 1 103 (April 1962).

7. H. Kouts, J. Nucl. Energy, 17 153 (July 1963).

8. E. Kreyszig, Advanced Engineering Math., 2nd ed., p. 763, John Wiley and Sons, Inc., New York, New York (1967).

9. W. G. Moffatt, G. W. Pearsall and J. Wulff, The Structure and Properties of Materials, Vol. 1, pp. 219-221, John Wiley and Sons, Inc., New York, New York (1964).

10. T. M. Sabine, J. D. Browne and J. L. Symonds, Australian J. Appl. Sci., 14 270 (May 1965).

11. H. J. Skank, Personal Communication (Nov. 1967).

12. R. G. Struss, "The Design and Operation of a Slow Neutron Chopper," M.S. Thesis, Iowa State University (1966).

ACKNOWLEDGMENTS

The author wishes to express his gratitude to his major professor, Dr. Richard Hendrickson, for his guidance and encouragement. The author also wishes to express his gratitude to Mr. Harold Skank and Mr. Roland Struss for their help and guidance in this work. In addition the author expresses appreciation to the Ames Laboratory (USAEC) for providing the funds and equipment for this study.

In conclusion, the author wishes to acknowledge his wife, Marlyn, for her efforts, encouragement and understanding during this study.

APPENDIX A. PROGRAM DATARE DESCRIPTION AND FLOW CHART

This section presents the description, flow chart and program listing for the DATARE program.

The flow chart for the DATARE program is given in Figure 21. The input and output parameters are defined as follows:

D	- Array of channel data
D2	- Array of channel data corrected for probability of detection
D4	- Array of final corrected spectrum data
D5	- Array of channel counts with total counts normalized to 1.00
E	- Array of energies corresponding to channels
EBAR	- Average energy in the region of interest
F1T, F2T, F3T	- The aperture correction functions for the appropriate time intervals
H	- Frequency input to chopper drive motor
I	- Array of input counts recorded per channel
N	- Total number of data channels
Q	- Channel width (micro-seconds)
T	- Array of flight times corresponding to channels
TC	- Total counts in energy range of interest
TV1, TV2, TV3, TV4	- Values of flight time bounding the aperture correction functions
U	- Flight path length (inches)
V	- Array of velocities corresponding to channels
VA	- Average velocity of the meaningful portion of the spectrum

X - Initial constant time interval

Y - Probability of detection

As indicated on the flow chart, the program reads and stores the input data, corrects for probability of detection and chopper aperture. The program also normalizes the data, calculates velocity, energy, time of flight, and prints out the data in a suitable format.

The program listing is given in Figure 22.

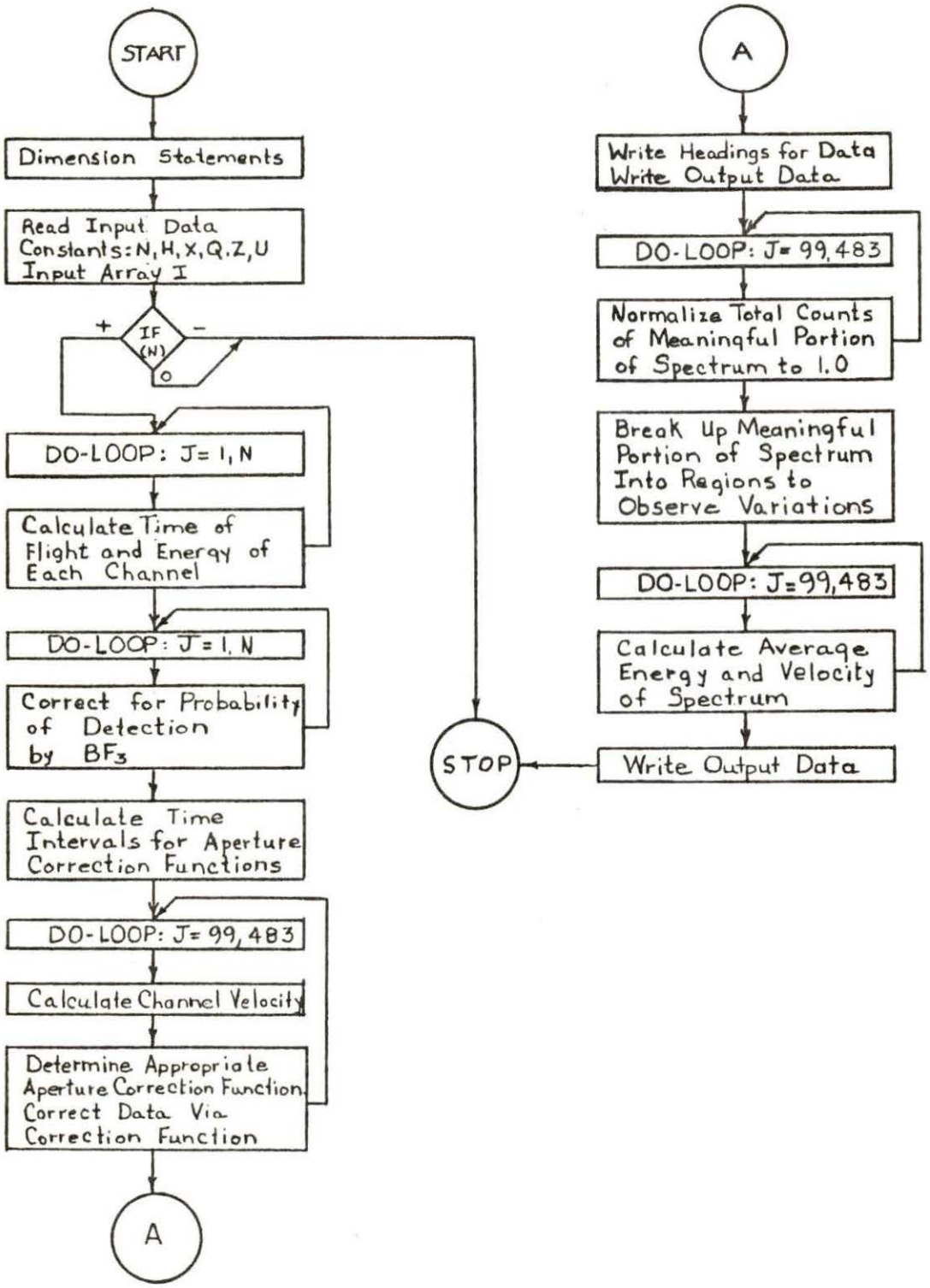

Figure 21. Flow chart for the DATARE computer program

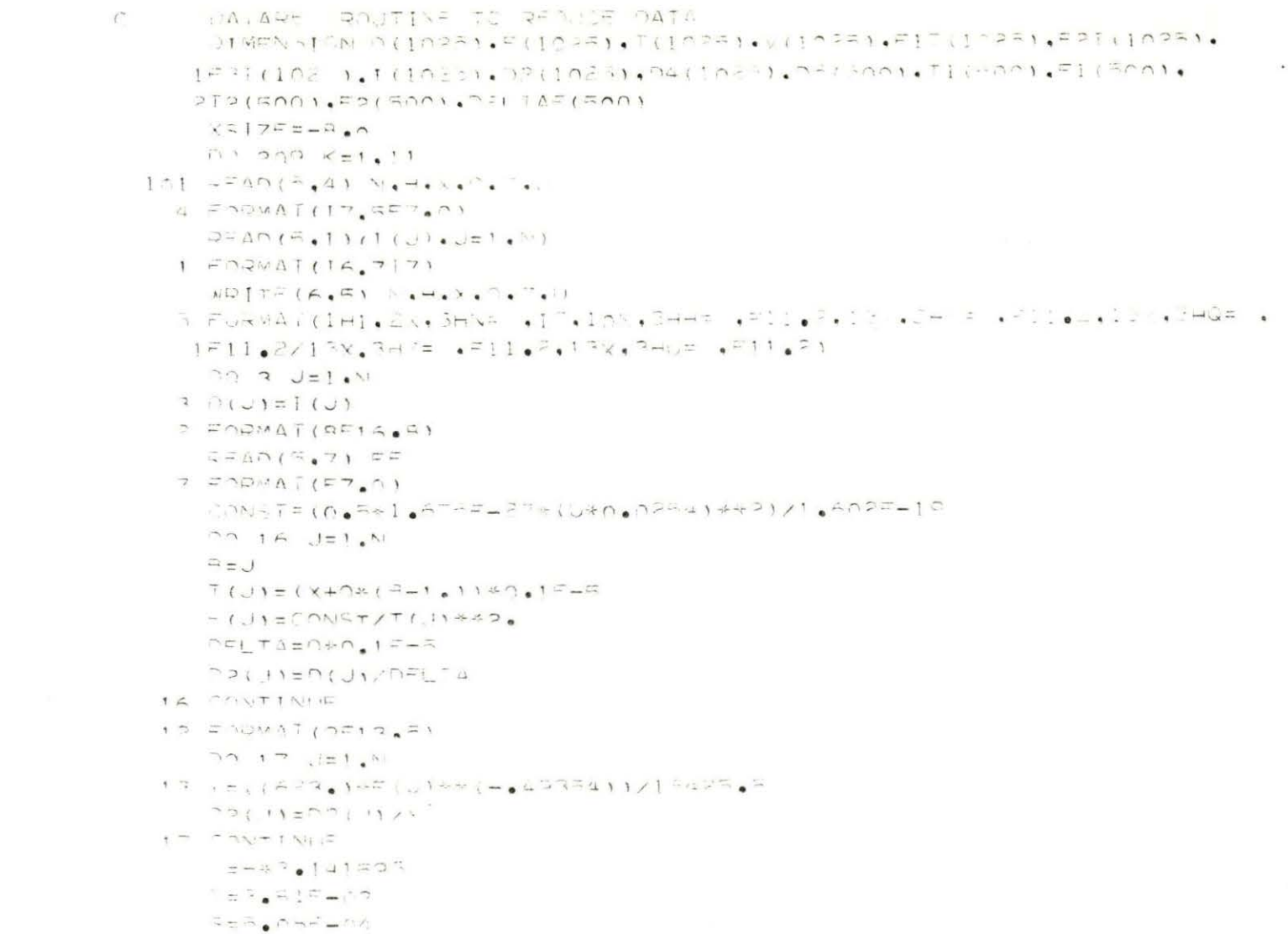

Figure 22. Listing of program DATARE

Figure 22. (Continued)

```
      WRITE(6,30)
   30 FORMAT(1H1,1X,2HJ ,5X,4HTIME,10X,8HVELOCITY,8X,6HENERGY,10X,
     114HBACKGROUND COR,3X,13H[illegible] CORRECTED,2X,15H[illegible] CRCTD.)
      WRITE(6,8) (J,T(J),V(J),E(J),D(J),D2(J),D4(J),J=29,483)
    8 FORMAT(I5,6E16.8)
   [illegible] FORMAT(9E13.5)
C     NORMALIZE TOTAL COUNTS TO 1.00
      TC=0.0
      DO 100 J=29,483
      TC=TC+D4(J)
  100 CONTINUE
      DO 102 J=29,483
      D5(J)=D4(J)/TC
  102 CONTINUE
      TC2=0.0
      DO 103 J=29,483
      TC2=TC2+D5(J)
  103 CONTINUE
      WRITE(6,105) (J,E(J),D5(J),J=29,483)
  105 FORMAT(5X,I5,2E16.5)
C     NORMALIZE COUNTS-ENERGY RANGE 0.4 -0.2165 (INF TO 5KT -- T=503 K )
      TC3=0.0
      DO 106 J=29,135
      TC3=TC3+D5(J)
  106 CONTINUE
C     NORMALIZE COUNTS-ENERGY RANGE  0.2165 - 0.0866 (5KT TO 2KT)
      TC4=0.0
      DO 107 J=136,213
      TC4=TC4+D5(J)
  107 CONTINUE
C     NORMALIZE COUNTS-ENERGY RANGE 0.0.0866-0.0433  (2KT TO KT)
      TC5=0.0
      DO 108 J=214,302
      TC5=TC5+D5(J)
  108 CONTINUE
```

Figure 22. (Continued)

```
C      NORMALIZE COUNTS-ENERGY RANGE 0.0483  - 0.01E-1 . KEV TO APP. 0 )
       TC6=0.0
       DO 109 J=303.483
       TC6=TC6+D6(J)
  109  CONTINUE
       SUM=0.0
       DO 201 J=99.483
       R7=J
       T1(J)=(Q*(R7-1.0))*0.1E-5
       E1(J)=CONST/T1(J)**2.
       T2(J)=((4.0+Q)*(R7-1.0))*0.1E-5
       E2(J)=CONST/T2(J)**2.
       DELTAE(J)=E1(J)-E2(J)
       SUM=SUM+(DELTAE(J)*D4(J))
  201  CONTINUE
       WRITE(6.104) TC.TC2.SUM
  104  FORMAT(1H1.3E16.8)
       WRITE(6.111) TC3.TC4.TC5.TC6
  111  FORMAT(1H1.9HREGION 4=.E16.8.10X.9HREGION 3=.E16.8/9HREGION 2=.
      1E16.8.10X.9HREGION 1=.E16.8)
       N1=0
       VN1=0.0
       VN11=0.0
       DO 91 J=99.483
       VN=V(J)*D4(J)
       VN1=VN1+VN
   91  VN11=VN11+D4(J)
       VA=VN1/VN11
       WRITE(6.92) VA
   92  FORMAT(1H1.E16.8)
       FRAD=0.0
       DO 200 J=99.483
  200  FRAD=FRAD+D4(J)*F(J)
       WRITE(6.92) FRAD
```

Figure 22. (Continued)

```
209 CONTINUE
    CALL EXIT
    END
```

CARDS 01-13-71 -1 5 002 26

Figure 22. (Continued)

APPENDIX B. DETERMINATION OF THE CHOPPER APERTURE CORRECTION AS A FUNCTION OF TIME

The neutron chopper aperture correction as a function of velocity will be derived first, since the correction as a function of time uses much of the same material [11].

The problem to be considered involves the operation of a Fermi type neutron chopper, and the development of the equations necessary to correct the data taken.

Suppose the availability of a neutron spectrum of velocities described by a probability function is $N(v,t)$, where $N(v,t)$ is the neutron population at velocity v and time t. At a reactor beam port the neutron spectrum should be independent of time, i.e. $\partial N(v,t)/\partial t = 0$.

The basic construction of the chopper used is illustrated in Figure 23. It is constructed of alternating laminations of cadmium and aluminum of length 2R and thickness W compressed together and rotated about the center point at angular velocity ω.

Figure 24 illustrates a single slit or "window" in the following positions: 1) starting to open; 2) full open; 3) just closed.

If we consider that one end of the turning "window" is exposed to a beam of collimated neutrons and that all neutrons passing through the "window" travel in straight line paths; then we may approximate the effect of the window by the two

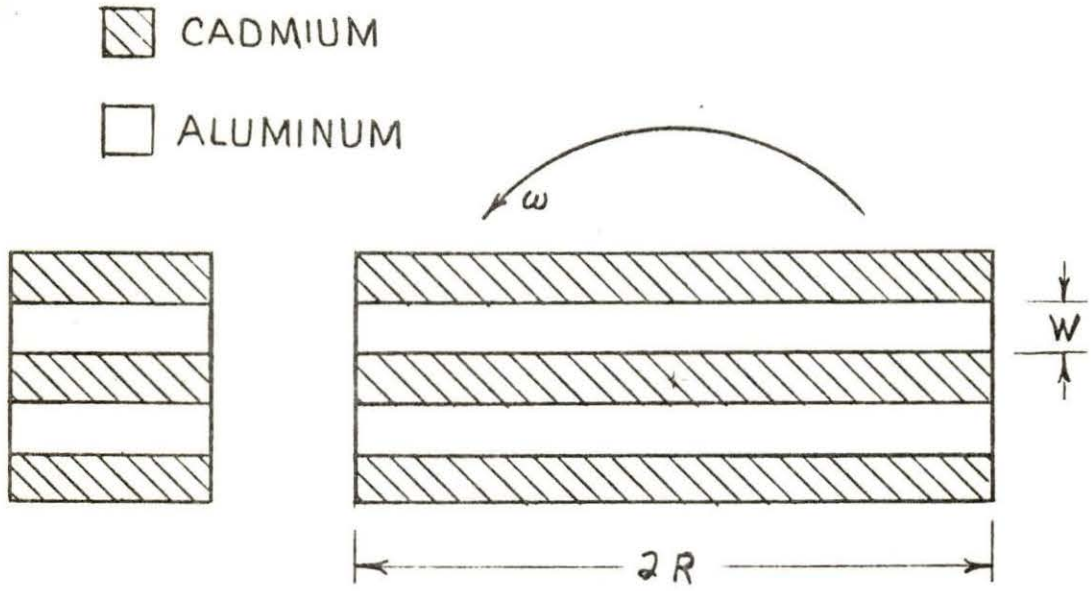

Figure 23. Illustrates basic construction of the chopper

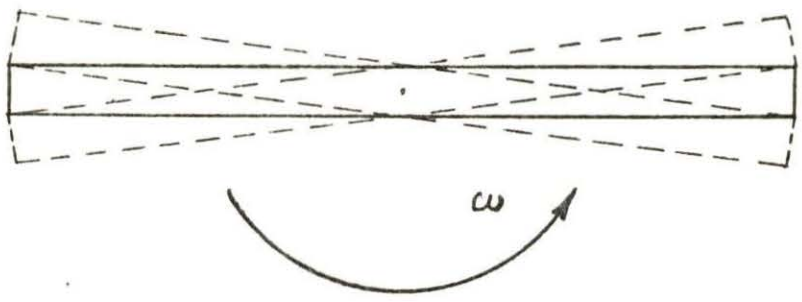

Figure 24. Illustration of a single rotating slit or window

shutters illustrated in Figure 25.

Assume that at time t = 0 the window is open or parallel to the collimated beam. Refer to Figure 25 for variable definitions.

Then: $x_1(0) = -\frac{W}{2}$

$$x_2(0) = \frac{W}{2}$$

$$x_1(t) = -\frac{W}{2} - \omega Rt$$

When $x_1(t) = \frac{W}{2}$ the window is opening.

Thus $\frac{W}{2} = -\frac{W}{2} - \omega Rt$

$$-\omega Rt = W$$

$$t = -\frac{W}{\omega R}$$

From Figure 25 it can be seen that

$$x_2(t) = x_1(t) + W.$$

Therefore $x_2(t) = \frac{W}{2} - \omega Rt$.

When $x_2(t) = -\frac{W}{2}$ the window is just closed.

Thus $-\frac{W}{2} = \frac{W}{2} - \omega Rt$

$$W = \omega Rt$$

$$t = \frac{W}{\omega R}$$

Similarly for area A_2

$$x_3(0) = \frac{W}{2}$$

Figure 25. Shutters illustrating window ends

Figure 26. (lower left) Effective area of transmission for $\frac{2\omega R^2}{W} \leq v$

Figure 27. (lower right) Effective area of transmission for $\frac{\omega R^2}{W} \leq v \leq \frac{2\omega R^2}{W}$

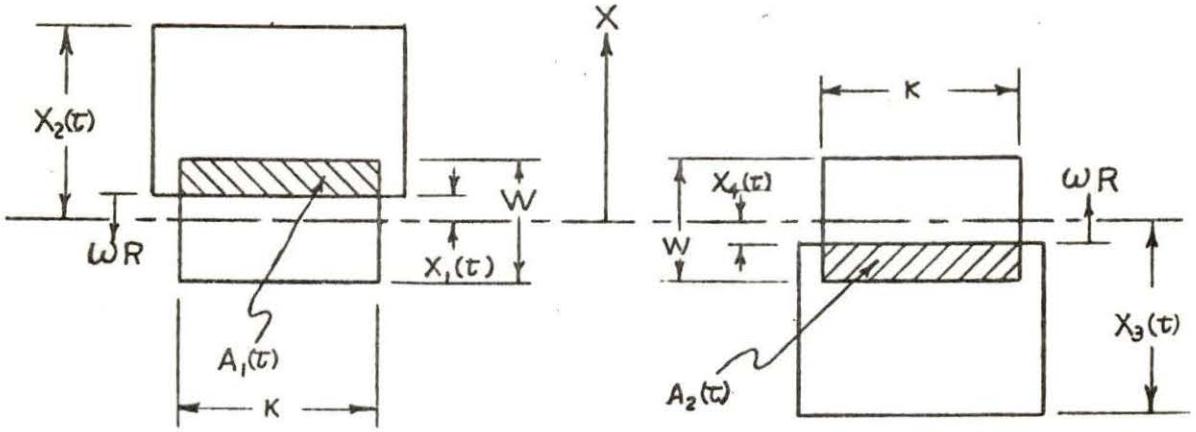
X
$X_2(\tau)$
ωR
W
$X_1(\tau)$
$A_1(\tau)$
K
K
$X_4(\tau)$
W
ωR
$X_3(\tau)$
$A_2(\tau)$

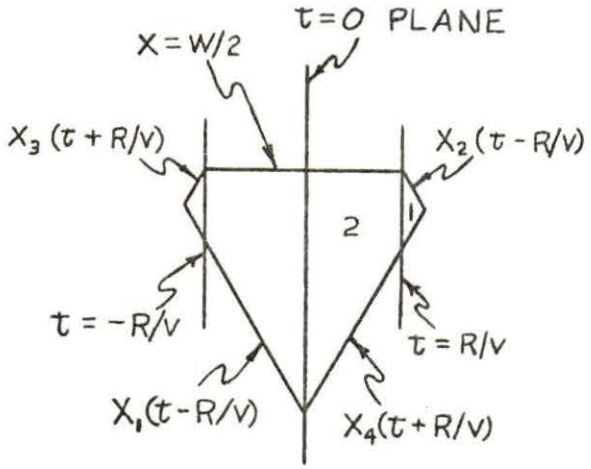
$\tau = 0$ PLANE
$X = W/2$
$X_3(\tau + R/V)$
$X_2(\tau - R/V)$
2
1
$\tau = -R/V$
$\tau = R/V$
$X_1(\tau - R/V)$
$X_4(\tau + R/V)$

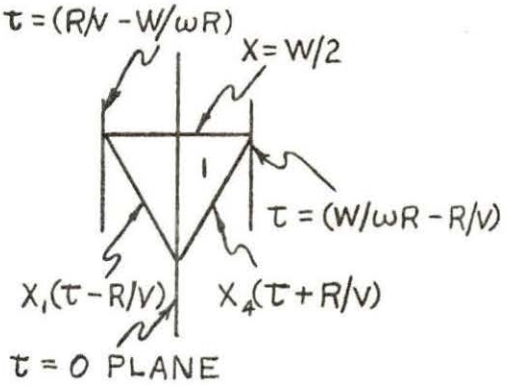
$\tau = (R/V - W/\omega R)$
$X = W/2$
1
$\tau = (W/\omega R - R/V)$
$X_1(\tau - R/V)$
$X_4(\tau + R/V)$
$\tau = 0$ PLANE

$$x_4(0) = -\frac{W}{2}$$

$$x_3(t) = \frac{W}{2} + \omega R t$$

$$x_4(t) = -\frac{W}{2} + \omega R t$$

Area $A_1(t)$ is bounded by:

$$x_1(t) \leq x \leq \frac{W}{2} \text{ for } -\frac{W}{\omega R} \leq t \leq 0$$

$$-\frac{W}{2} \leq x \leq x_2(t) \text{ for } 0 \leq t \leq \frac{W}{\omega R}$$

It is preferable to describe the boundary edges of the neutrons passing through Area A_1 by delaying the area A_1 by the time corresponding to the time necessary to travel a distance R.

$$A_1(t) \text{ delayed} = A_1(t - \frac{R}{v})$$

$$A_1(t - \frac{R}{v}) \text{ is bounded by } \omega R(\frac{R}{v} - t) - \frac{W}{2} \leq x \leq \frac{W}{2}$$

$$\text{and } -\frac{W}{2} \leq x \leq \omega R(\frac{R}{v} - t) + \frac{W}{2}$$

Thus $x_1(t-\frac{R}{v}) = \omega R(\frac{R}{v}-t) - \frac{W}{2}$ and $x_2(t-\frac{R}{v}) = \omega R(\frac{R}{v}-t) + \frac{W}{2}$

Simultaneously area A_2 can be expressed as being bounded by:

$$-\frac{W}{2} \leq x \leq \frac{W}{2} + \omega R t \text{ for } -\frac{W}{\omega R} \leq t \leq 0$$

$$-\frac{W}{2} + \omega R t \leq x \leq \frac{W}{2} \text{ for } 0 \leq t \leq \frac{W}{\omega R}$$

To provide a convenient point of reference, area A_2 will be shifted earlier in time by R/v to provide a space reference point at the center of the chopper.

Thus $A_2(t+\frac{R}{v})$ is bounded by:

$$-\frac{W}{2} \leq x \leq \omega R(\frac{R}{v}+t) + \frac{W}{2}$$

and

$$\omega R(\frac{R}{v}+t) - \frac{W}{2} \leq x \leq \frac{W}{2}$$

Thus

$$x_3(t+\frac{R}{v}) = \omega R(\frac{R}{v}+t) + \frac{W}{2}$$

$$x_4(t+\frac{R}{v}) = \omega R(\frac{R}{v}+t) - \frac{W}{2}$$

By substituting values it can be shown that the effective area for transmission takes the shape of Figure 26 for $2\omega R^2/W \leq v$ and Figure 27 for $\omega R^2/W \leq v \leq 2\omega R^2/W$.

For $x_1(t-\frac{R}{v}) = \frac{W}{2}$ the window is opening.

Thus $\omega R(\frac{R}{v}-t) - \frac{W}{2} = \frac{W}{2}$

$$\omega R(\frac{R}{v}-t) = W$$

$$t = \frac{R}{v} - \frac{W}{\omega R}$$

For $x_4(t+\frac{R}{v}) = \frac{W}{2}$ the window is closing.

Thus $\omega R(\frac{R}{v}+t) - \frac{W}{2} = \frac{W}{2}$

$$\frac{R}{v} + t = \frac{W}{\omega R}$$

$$t = \frac{W}{\omega R} - \frac{R}{v}$$

The value of v at the intersection of x_1 and x_4 is the limiting or cut-off velocity $v_{c.o.}$.

$$\frac{R}{v} - \frac{W}{\omega R} = \frac{W}{\omega R} - \frac{R}{v}$$

$$\frac{R}{v} = \frac{W}{\omega R}$$

$$v = \frac{\omega R^2}{W} = v_{c.o.}$$

The values of t when x_2 and x_3 intersect the W/2 plane are:

$$x_2(t-\frac{R}{v}) = \frac{W}{2} \qquad x_3(t+\frac{R}{v}) = \frac{W}{2}$$

$$\omega R(\frac{R}{v}-t) + \frac{W}{2} = \frac{W}{2} \qquad \omega R(\frac{R}{v}+t) + \frac{W}{2} = \frac{W}{2}$$

$$t = \frac{R}{v} \qquad t = -\frac{R}{v}$$

For the outside edges in time of Figure 26.

$$x_3(t+\frac{R}{v}) = x_1(t-\frac{R}{v})$$

$$\omega R(\frac{R}{v}+t)+\frac{W}{2} = \omega R(\frac{R}{v}-t) - \frac{W}{2}$$

$$2\omega Rt = -W$$

$$t = \frac{-W}{2\omega R}$$

Likewise for $x_4(t+\frac{R}{v}) = x_2(t-\frac{R}{v})$

$$\omega R(\frac{R}{v}+t)-\frac{W}{2} = \omega R(\frac{R}{v}-t) + \frac{W}{2}$$

$$2\omega Rt = W$$

$$t = \frac{W}{2\omega R}$$

Now to compute the values for effective window width as a function of time and velocity.

For Figure 26 (i.e. $\frac{2\omega R^2}{W} \leq v \leq \infty$)

$$x_3 - x_1 = [\omega R(\frac{R}{v}+t)+\frac{W}{2}] - [\omega R(\frac{R}{v}-t)-\frac{W}{2}] = W+2\omega Rt$$

$$\text{for } -\frac{W}{2\omega R} \leq t \leq -\frac{R}{v}$$

$$\frac{W}{2} - x_1 = \frac{W}{2} - [\omega R(\frac{R}{v}-t)-\frac{W}{2}] = W+\omega Rt-\frac{\omega R^2}{v}$$

$$\text{for } -\frac{R}{v} \leq t \leq 0$$

$x_c(v,t) =$

$$\frac{W}{2} - x_4 = \frac{W}{2} - [\omega R(\frac{R}{v}+t)-\frac{W}{2}] = W-\omega Rt-\frac{\omega R^2}{v}$$

$$\text{for } 0 \leq t \leq \frac{R}{v}$$

$$x_2 - x_4 = [\omega R(\frac{R}{v}-t)+\frac{W}{2}] - [\omega R(\frac{R}{v}+t)-\frac{W}{2}] = W-2\omega Rt$$

$$\text{for } \frac{R}{v} \leq t \leq \frac{W}{2\omega R}$$

Likewise for Figure 27 (i.e. $\frac{\omega R^2}{W} \leq v \leq \frac{2\omega R^2}{W}$)

$$\frac{W}{2} - x_1 = W+\omega Rt - \frac{\omega R^2}{v} \quad \text{for } \frac{R}{v} - \frac{W}{\omega R} \leq t \leq 0$$

$$\frac{W}{2} - x_4 = W-\omega Rt - \frac{\omega R^2}{v} \quad \text{for } 0 \leq t \leq \frac{W}{\omega R} - \frac{R}{v}$$

$x_c(v,t)$ may be visualized as the height of the region at the center of a given slit through which a neutron of velocity v must pass at the time t in order to travel completely through the chopper "window". Thus the probability of finding neutrons of velocity v that will pass through the chopper is a function of time, and is equal to:

$$P(v,t) = N(v)Kx_c(v,t)$$

The aperture correction used is derived from the assumption that all the neutrons of a certain velocity are grouped closely together in time at the detector, thereby permitting their normalization according to an attenuation function.

The number of neutrons of a given velocity that pass the chopper is proportional to $x_c(v,t)$, and proportional to the length of time associated with $x_c(v,t)$. Therefore, if the aperture function of velocity is $F(v)$, then: $dF(v) = dx_c dt$.

$F(v) = \int\int dx_c dt$, which corresponds to the cross-sectional area of our figure. Thus, for $2\omega R^2/W \leq v$ the area of section 1 in Figure 26 is $A_1 = 1/2\ bh$ where $b = (W/2\omega R - R/v)$ and $h = W - 2\omega Rt|_{t=R/v}, h = W - 2\omega R^2/v$. Therefore

$$A_1 = 1/2\left(\frac{W}{2\omega R}-\frac{R}{v}\right)\left(W-\frac{2\omega R^2}{v}\right) = \omega R\left(\frac{W}{2\omega R}-\frac{R}{v}\right)^2$$

For the area of section 2 Figure 26

$$A_2 = 1/2\left(\frac{R}{v}\right)\left(W-\frac{2\omega R^2}{v} + W - \frac{\omega R^2}{v}\right)$$

$$= \frac{R}{2v}\left(2W-\frac{3\omega R^2}{v}\right) = \omega R\left(\frac{W}{\omega v}-\frac{3R^2}{2v^2}\right)$$

Due to symmetry about the t=0 plane,

$$F(v) = 2(A_1+A_2) = 2\omega R\left(\frac{W^2}{4\omega^2R^2}-\frac{R^2}{2v^2}\right) \text{ for } \frac{2\omega R^2}{W} \leq v$$

For $\frac{\omega R^2}{W} \leq v \leq \frac{2\omega R^2}{W}$ area A_1 in Figure 27 is:

$$A_1 = 1/2\left(\frac{W}{\omega R}-\frac{R}{v}\right)\left(W-\frac{\omega R^2}{v}\right) = \frac{\omega R}{2}\left(\frac{W}{\omega R}-\frac{R}{v}\right)^2$$

Thus $F(v) = 2A_1 = \omega R(\frac{W}{\omega R}-\frac{R}{v})^2$ for $\frac{\omega R^2}{W} \leq v \leq \frac{2\omega R^2}{W}$

It proves beneficial to normalize this function to the function at infinite velocity $F(\infty)$ where

$$F(\infty) = 2\omega R(\frac{W^2}{4\omega^2R^2}-\frac{R^2}{2\infty^2}) = 2\omega R(\frac{W^2}{4\omega^2R^2})$$

$$= \frac{W^2}{2\omega R}$$

for $\frac{2\omega R^2}{W} \leq v$ $\quad \frac{F(v)}{F(\infty)} = 1 - 2(\frac{\omega R^2}{vW})^2$

And for $\frac{\omega R^2}{W} \leq v \leq \frac{2\omega R^2}{W}$ $\quad \frac{F(v)}{F(\infty)} = 2(1-\frac{\omega R^2}{vW})^2$

Let $F_1(v) = \frac{F(v)}{F(\infty)}$, then

$F_1(v) = 0$ for $0 \leq v \leq \frac{\omega R^2}{W}$

$F_1(v) = 2(1-\frac{\omega R^2}{vW})^2$ for $\frac{\omega R^2}{W} \leq v \leq \frac{2\omega R^2}{W}$

$F_1(v) = 1-2(\frac{\omega R^2}{vW})^2$ for $\frac{2\omega R^2}{W} \leq v \leq \infty$

Thus, $F_1(v)$ is the aperture correction function.

We now compute the neutron population as a function of t and v at the detector.

From page 75 for $\frac{2\omega R^2}{W} \leq v \leq \infty$

$$x_c(v,t) = W + 2\omega Rt \qquad \text{for } -\frac{W}{2\omega R} \leq t \leq -\frac{R}{v}$$

$$x_c(v,t) = W + \omega Rt - \frac{\omega R^2}{v} \qquad \text{for } -\frac{R}{v} \leq t \leq 0$$

$$x_c(v,t) = W - \omega Rt - \frac{\omega R^2}{v} \qquad \text{for } 0 \leq t \leq \frac{R}{v}$$

$$W - 2\omega Rt \qquad \text{for } \frac{R}{v} \leq t \leq \frac{W}{2R}$$

Likewise for $\frac{\omega R^2}{W} \leq v \leq \frac{2\omega R^2}{W}$

$$x_c(v,t) = W + \omega Rt - \frac{\omega R^2}{v} \qquad \text{for } \frac{R}{v} - \frac{W}{\omega R} \leq t \leq 0$$

$$x_c(v,t) = W - \omega Rt - \frac{\omega R^2}{v} \qquad \text{for } 0 \leq t \leq \frac{W}{\omega R} - \frac{R}{v}$$

For $0 \leq v \leq \frac{\omega R^2}{W}$

$$x_c(v,t) = 0$$

The distance from the center of the chopper to the detector is defined as D. We now compute $x_c(v,t - \frac{D}{v}) = x_d(v,t)$.

For $\frac{2\omega R^2}{W} \leq v \leq \infty$

$$x_d(v,t) = W + 2\omega Rt - \frac{2\omega RD}{v} \qquad \text{for } \frac{D}{v} - \frac{W}{2\omega R} \leq t \leq \frac{D-R}{v}$$

$$x_d(v,t) = W + \omega Rt - \frac{\omega R}{v}(D+R) \qquad \text{for } \frac{D-R}{v} \leq t \leq \frac{D}{v}$$

$$x_d(v,t) = W - \omega Rt + \frac{\omega R}{v}(D-R) \qquad \text{for } \frac{D}{v} \leq t \leq \frac{D+R}{v}$$

$$x_d(v,t) = W - 2\omega Rt + \frac{2\omega RD}{v} \qquad \text{for } \frac{D+R}{v} \leq t \leq \frac{D}{v} + \frac{W}{2\omega R}$$

Likewise for $\frac{\omega R^2}{W} \leq v \leq \frac{2\omega R^2}{W}$

$$x_d(v,t) = W + \omega Rt - \frac{\omega R}{v}(D+R) \qquad \text{for } \frac{R+D}{v} - \frac{W}{\omega R} \leq t \leq \frac{D}{v}$$

$$x_d(v,t) = W - \omega Rt + \frac{\omega R}{v}(D-R) \qquad \text{for } \frac{D}{v} \leq t \leq \frac{W}{\omega R} + \frac{D-R}{v}$$

And for $0 \leq v \leq \frac{\omega R^2}{W}$

$$x_d(v,t) = 0$$

To observe the intersections of the various x_d's, we simply substitute values of v into the boundary values of time (i.e. values of v into $t = D/v - W/2\omega R$, $t = D-R/v$, $t = D/v$ etc.). The resultant intersections of $x_d(v,t)$ are plotted in Figure 28.

In the velocity dispersion shown in Figure 28, data recorded before $t = W/2\omega R$ includes infinite velocity neutrons. For the moment let us drop all data where $t \leq W/2\omega R$.

$$\text{For } t_1 = \frac{D}{v} - \frac{W}{2\omega R}\Big|_{v=\frac{2\omega R^2}{W}} = \frac{W}{2\omega R}\left(\frac{D}{R}-1\right),$$

values of $D/R > 2$ give values of $t_1 > W/2\omega R$. Therefore, we are interested in values of t greater than t_1.

$$\Delta v(t) = v_{MAX}(t) - v_{MIN}(t)$$

$$t = \frac{D}{v_{MAX}} + \frac{W}{2\omega R} \; ; \; v_{MAX} = \frac{D}{t - \frac{W}{2\omega R}}$$

$$t = \frac{D}{v_{MIN}} - \frac{W}{2\omega R} \; ; \; v_{MIN} = \frac{D}{t + \frac{W}{2\omega R}}$$

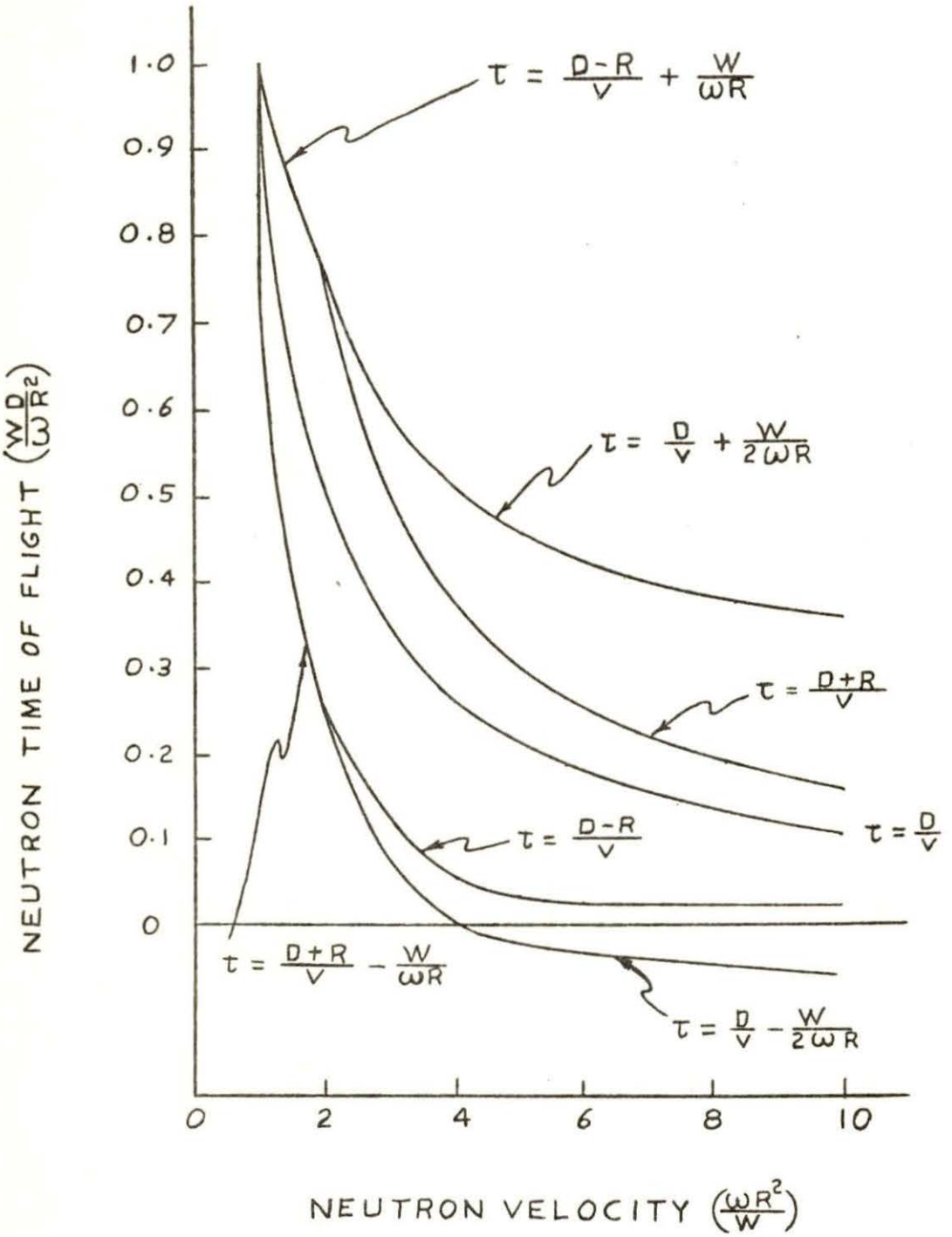

Figure 28. Representation of a velocity dispersion showing the limits in time and velocity for the functions

$$\Delta v(t) = D\left[\frac{1}{t - \frac{W}{2\omega R}} - \frac{1}{t + \frac{W}{2\omega R}} \right]$$

The most probable velocity in this increment is $v = D/t$.

Consider now the computation of the following integral.

$$F(t) = \int_{v_{MIN}}^{v_{MAX}} x_d(v,t)\,dv$$

To cover the whole range of possible values the above integral must be calculated in four sections.

1) $-\frac{W}{2\omega R} \leq t \leq \frac{W}{2\omega R}$, for $v_{MAX} = \infty$, $v_{MIN} = \frac{D}{t + \frac{W}{2\omega R}}$

2) $\frac{W}{2\omega R} \leq t \leq \frac{W}{2\omega R}(\frac{D}{R}-1)$, for $v_{MAX} = \frac{D}{t - \frac{W}{2\omega R}}$, $v_{MIN} = \frac{D}{t + \frac{W}{2\omega R}}$

3) $\frac{W}{2\omega R}(\frac{D}{R}-1) \leq t \leq \frac{W}{2\omega R}(\frac{D}{R}+1)$, for $v_{MAX} = \frac{D}{t - \frac{W}{2\omega R}}$, $v_{MIN} = \frac{D}{t + \frac{W}{2\omega R}}$

4) $\frac{W}{2\omega R}(\frac{D}{R}+1) \leq t \leq \frac{WD}{\omega R^2}$, for $v_{MAX} = \frac{D-R}{t - \frac{W}{\omega R}}$, $v_{MIN} = \frac{D+R}{t + \frac{W}{\omega R}}$

For section 1 (i.e., $-\frac{W}{2\omega R} \leq t \leq \frac{W}{2\omega R}$) the integral

$F(t) = \int_{v_{MIN}}^{\infty} x_d(v,t)\,dv$ is

$$F(t) = \int_{v_{MIN}}^{\infty} (W + 2\omega Rt - \frac{2\omega RD}{v})\,dv$$

$$= (W+2\omega Rt)v - 2\omega RD \ln v \Big|_{\frac{D}{t+\frac{W}{2\omega R}}}^{\infty}$$

$$= \infty$$

Performing the integral for $\frac{W}{2\omega R} \leq t \leq \frac{W}{2\omega R}(\frac{D}{R}-1)$ we have

$$F_1(t) = \int_{t+\frac{W}{2\omega R}}^{\frac{D-R}{t}} (W+2\omega Rt-\frac{2\omega RD}{v})dv + \int_{\frac{D-R}{t}}^{D/t} [W+\omega Rt-\frac{\omega R}{v}(D+R)]dv$$

$$+\int_{D/t}^{\frac{D+R}{t}} [W-\omega Rt+\frac{\omega R(D-R)}{v}]dv + \int_{\frac{D+R}{t}}^{\frac{D}{t-\frac{W}{2\omega R}}} (W-2\omega Rt+\frac{2\omega RD}{v})dv$$

which reduces to;

$$F_1(t) = WD[\frac{1}{t-\frac{W}{2\omega R}} - \frac{1}{t+\frac{W}{2\omega R}}] + 2\omega RDt[\frac{2}{t} - \frac{1}{t-\frac{W}{2\omega R}} - \frac{1}{t+\frac{W}{2\omega R}}]$$

$$+2\omega RD \ln\left\{\frac{D^2t^2}{(D^2-R^2)[t^2-(\frac{W}{2\omega R})^2]}\right\} + \omega RD \ln(\frac{D^2-R^2}{D^2}) - \omega R^3 \ln\frac{D+R}{D-R}$$

For the next region: $\frac{W}{2\omega R}(\frac{D}{R}-1) \leq t \leq \frac{W}{2\omega R}(\frac{D}{R}+1)$

$$F_2(t) = \int_{t+\frac{D+R}{\omega R}}^{D/t} [W+\omega Rt-\frac{\omega R(D+R)}{v}]dv + \int_{D/t}^{\frac{D+R}{t}} [W-\omega Rt+\frac{\omega R(D-R)}{v}]dv$$

$$+\int_{\frac{D+R}{t}}^{\frac{D}{t-\frac{W}{2\omega R}}} [W-2\omega Rt+\frac{2\omega RD}{v}]dv$$

which reduces to;

$$F_2(t) = W(\frac{D}{t-\frac{W}{2\omega R}} - \frac{D+R}{t+\frac{W}{\omega R}}) + \omega R(3D+R) - \omega Rt(\frac{D+R}{t+\frac{W}{\omega R}} + \frac{2D}{t-\frac{W}{2\omega R}})$$

$$+ \omega RD \ln(\frac{t^3}{(t+\frac{W}{\omega R})(t-\frac{W}{2\omega R})^2}) + \omega R^2 \ln(\frac{t}{t+\frac{W}{\omega R}})$$

For the last region: $\frac{W}{2\omega R}\left(\frac{D}{R}+1\right) \leq t \leq \frac{WD}{\omega R^2}$

$$F_3(t) = \int_{t+\frac{W}{\omega R}}^{D/t} \left[W+\omega Rt-\frac{\omega R(D+R)}{v}\right]dv + \int_{D/t}^{t-\frac{W}{\omega R}} \left[W-\omega Rt+\frac{\omega R(D-R)}{v}\right]dv$$

which reduces to;

$$F_3(t) = W\left(\frac{D-R}{t-\frac{W}{\omega R}} - \frac{D+R}{t+\frac{W}{\omega R}}\right) + 2\omega RD - \omega Rt\left(\frac{D-R}{t-\frac{W}{\omega R}} + \frac{D+R}{t+\frac{W}{\omega R}}\right)$$

$$+ \omega RD \ln \frac{(D^2-R^2)t}{D^2\left[t^2-\left(\frac{W}{\omega R}\right)^2\right]} + \omega R^2 \ln \frac{(D+R)\left(t-\frac{W}{\omega R}\right)}{(D-R)\left(t+\frac{W}{\omega R}\right)}$$

The following checks were worked out algebraically and found to agree.

$$F_3(t) = 0 \qquad \text{at } t = \frac{WD}{\omega R^2}$$

$$F_3(t) = F_2(t) \qquad \text{at } t = \frac{W}{2\omega R}\left(\frac{D}{R}+1\right)$$

$$F_2(t) = F_1(t) \qquad \text{at } t = \frac{W}{2\omega R}\left(\frac{D}{R}-1\right)$$

The composite function appears below:

For $\frac{W}{2\omega R} < t \leq \frac{W}{2\omega R}(\frac{D}{R}-1)$,

$$F(t) = W(\frac{D}{t-\frac{W}{2\omega R}} - \frac{D}{t+\frac{W}{2\omega R}}) + 4\omega RD - 2\omega Rt(\frac{D}{t-\frac{W}{2\omega R}} + \frac{D}{t+\frac{W}{2\omega R}})$$

$$-\omega RD \ln\frac{D^2}{D^2-R^2} - \omega R^2 \ln\frac{D+R}{D-R} + 2\omega RD \ln\frac{D^2t^2}{(D^2-R^2)[t^2-(\frac{W}{2\omega R})^2]},$$

for $\frac{W}{2\omega R}(\frac{D}{R}-1) \leq t \leq \frac{W}{2\omega R}(\frac{D}{R}+1)$,

$$F(t) = W(\frac{D}{t-\frac{W}{2\omega R}} - \frac{D+R}{t+\frac{W}{\omega R}} + \omega R(3D+R) - \omega Rt(\frac{2D}{t-\frac{W}{2\omega R}} + \frac{D+R}{t+\frac{W}{\omega R}})$$

$$+ \omega RD \ln\frac{t^3}{(t-\frac{W}{2\omega R})^2(t+\frac{W}{\omega R})} - \omega R^2 \ln\frac{t+\frac{W}{\omega R}}{t},$$

and for $\frac{W}{2\omega R}(\frac{D}{R}+1) \leq t \leq \frac{WD}{\omega R^2}$,

$$F(t) = W(\frac{D-R}{t-\frac{W}{\omega R}} - \frac{D+R}{t+\frac{W}{\omega R}}) + 2\omega RD - \omega Rt(\frac{D-R}{t-\frac{W}{\omega R}} + \frac{D+R}{t+\frac{W}{\omega R}})$$

$$- \omega RD \ln\frac{D^2[t^2-(\frac{W}{\omega R})^2]}{(D^2-R^2)t^2} - \omega R^2 \ln\frac{(D-R)(t+\frac{W}{\omega R})}{(D+R)(t-\frac{W}{\omega R})}.$$

Figure 29 shows the effective slit width as a function of time and velocity.

The counts received in a time increment at the detector correspond to the following:

$$C_i = k\int_{t_i}^{t_{i+1}} \int_{v_{MIN}}^{v_{MAX}} N(v)P_{DET}(v)x_d(v,t)dv\ dt$$

Where

C_i = counts/channel

$N(v)$ = neutron density in neutrons/square area

k = width of the chopper (or collimator) window

$P_{DET}(v)$ = detector efficiency as a velocity function

For the time region $t \geq 5W/\omega R$, the velocity variation for v in the above integral changes, less than $\pm 5\%$; thus a reasonable approximation is:

$$C_i = k\int_{t_i}^{t_{i+1}} N(V_{avg})P_{DET}(v_{avg})\int_{v_{MIN}}^{v_{MAX}} x_d(v,t)dv\ dt$$

however this is

$$C_i = kN(v_{avg})P_{DET}(v_{avg})\int_{t_i}^{t_{i+1}} F(t)dt,$$

and for sufficiently small time increments this becomes

$$C_i = kN(v_{avg})P_{DET}(v_{avg})F(t_{avg})\Delta t$$

and we arrive at

$$N(v_{avg}) = \frac{C_i}{kP_{DET}(v_{avg})F(t_{avg})\Delta t}$$

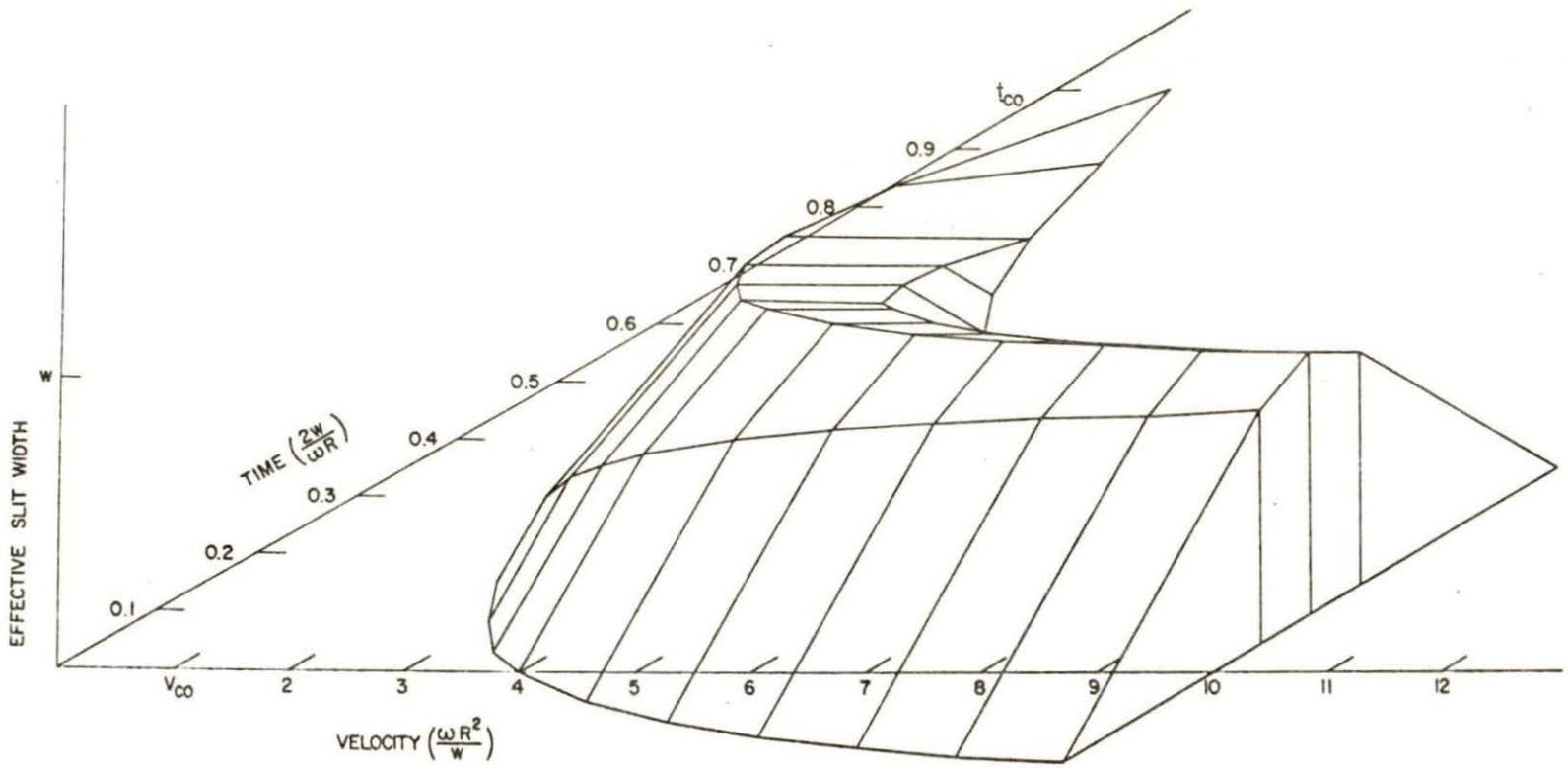

Figure 29. Effective area of transmission for neutrons with velocity v to pass through the chopper in time t

APPENDIX C. ERROR ANALYSIS

Discussion

In any experiment there will inevitably be some errors associated with the equipment and/or procedure used. The method of error analysis employed here was to determine the maximum reasonable deviation of the parameter studied, and to determine the effects of this deviation throughout the energy spectrum, using the computer program where possible. The reference case data for the error analysis was obtained after careful alignment of the experimental equipment without anything in the beam tube to modify the beam. In general the more pessimistic value of the parameter was used for the analysis; thus, the resultant error bar was larger than otherwise might be determined.

The following are the parameters studied and their effects. The individual errors are the difference between the reference case and the case with the varied parameter. The energy difference or error was determined by noting the variation from the aluminum scattering peaks.

Effect of time delay shift

There was approximately 4 micro-seconds time delay due to loss in cable, pulse-shaping electronics, and time of flight analyzer.

The start of "open" pulse was calibrated periodically; however, an error of $\pm$ 5 minutes of rotation was possible.

The ± 5 minutes of rotation would be an upper bound since the chopper "window" was only open for 59 minutes of rotation.

The input frequency of the chopper drive motor was 100 Hertz. This figure corresponds to 3000 rpm or 50 rps. There are 360 x 60 = 21,600 min/rev. (50 rev/sec) x (21,600 min/rev) = 1,080,000 min/sec, therefore

$$\frac{\pm\ 5 \text{ min}}{1.08 \times 10^{6} \text{ min/sec}} = \pm\ 4.63 \times 10^{-6} \text{ sec.}$$

The total time shift is 4 ± 4.63 microseconds or +8.63 microseconds and -0.63 microseconds (with a delay defined as positive). This value was then added to the constant (x in the computer program) in the equation used to determine the location of each channel in time.

Table C 1 gives the data and differences observed.

Effect of flight path variation

The flight path length was measured for each accumulation of spectrum data. The error in this measurement should be no greater than ± 1/4". Also, the size of the detector was assumed to be zero inches. The actual effective diameter of the detector was 0.875 inches. The effective change in flight length due to detector size was ± (0.5)(.875/2) = ± 0.22". Therefore, in error analysis the flight length was taken as ± 0.47 inches.

Table C 2 gives the data and differences observed.

Table C 1. Effect of variation in time delay

Reference value x 10^{-10} and energy (eV)	Observed value x 10^{-10} and energy (ev) for TD=8.63 μs	Observed value x 10^{-10} and energy (ev) for TD=-.63 μs	Difference for TD=8.63 μs	Difference for TD=-0.63 μs
39.25	39.5	38.25	+0.25	-0.40
0.02	0.01970	0.02025	-0.0003	+0.00025
46.4	46.65	46.1	+0.25	-0.30
0.03	0.02975	0.0302	-0.00025	+0.0002
48.5	48.75	48.2	+0.25	-0.30
0.04	0.0398	0.04015	-0.0002	+0.00015
45.8	46.25	45.75	+0.45	-0.05
0.06	0.0599	0.0601	-0.0001	+0.0001
40.5	40.35	40.6	-0.15	+0.10
0.08	0.08	0.08	0	0
33.0	32.75	33.15	-0.25	+0.15
0.10	0.10	0.10	0	0
13.8	13.75	14.0	-0.05	+0.20
0.20	0.20	0.20	0	0
9.75	9.70	9.75	-0.05	0
0.30	0.30	0.30	0	0

Table C 2. Effect of variation in flight path length

Reference value x 10^{-10} and energy (ev)	Observed value x 10^{-10} and energy (ev) for flight length +0.47"	Observed value x 10^{-10} and energy (ev) for flight length -0.47"	Difference for flight length +0.47"	Difference for flight length -0.47"
39.25	38.5	38.80	-0.75	-0.45
0.03	0.02035	0.02	+0.00035	0
46.4	45.75	46.1	-0.65	-0.30
0.03	0.0303	0.03	+0.0003	0
48.5	47.90	48.2	-0.60	-0.30
0.04	0.04025	0.04	+0.00025	0
45.8	45.7	45.7	-0.10	-0.10
0.06	0.06015	0.06	+0.00015	0
40.5	40.6	40.25	+0.10	-0.25
0.08	0.0801	0.08	+0.0001	0
33.0	33.15	32.65	+0.15	-0.35
0.10	0.10	0.10	0	0
13.8	14.0	13.8	+0.20	0
0.20	0.20	0.20	0	0
9.75	9.80	9.75	+0.05	0
0.30	0.30	0.30	0	0

Effect of dead time

The error caused by dead time of the system was controlled by the BF_3 detector used, since it has the longest recovery time of ten microseconds.

The following is a typical calculation used to determine the error caused by dead time. The shortest data accumulation time was 3.5 hours. The individual data channel widths used were 4 microseconds. At an energy of 0.08 eV, 9.644×10^3 counts were recorded. The chopper was revolving at 50 rev/sec, and there are two neutron bursts per revolution. In each data channel the data was accumulated for 8 μs/rev. In 3.5 hours there are 210 minutes. Therefore:

$$\frac{9.644 \times 10^3 \text{ counts}}{210 \text{ min}} = 45.92 \text{ counts/min}$$

$$\text{The equivalent counts/min} = \frac{45.92 \text{ CPM}}{(50\frac{\text{rev}}{\text{sec}})(8\times10^{-6}\ \frac{\text{sec}}{\text{rev}})} = 114{,}810 \text{ CPM}$$

$$R^1 = \frac{R}{1 - \tau R}$$

$$\tau = \frac{10\times10^{-6} \text{ sec}}{60 \text{ sec/min}} = 1.67\times10^{-7} \text{ min}$$

where: R^1 = actual count rate

R = observed count rate

τ = detector dead time

Therefore:

$$R^1 = \frac{1.1481\times10^5}{1-(1.1481\times10^5)(1.67\times10^{-7})} = \frac{1.1485\times10^5}{1 - 0.0192} = 1.171\times10^5 \text{ CPM}$$

$$\text{Percentage error} = \frac{(1.171-1.1485)\times10^5\times100}{1.171\times10^5} = 1.92\%$$

Table C 3 tabulates the error versus energy.

Table C 3. Effect of detector dead time

Neutrons energy (eV)	Observed counts	Actual count rate (CPM)	% error	Error value $\times10^{-10}$
0.02	3.07×10^3	3.6821×10^4	0.6	0.0576
0.03	5.59×10^3	6.73×10^4	1.11	0.2652
0.04	7.38×10^3	8.9171×10^4	1.5	0.507
0.06	9.26×10^3	1.123×10^5	1.8	0.710
0.08	9.644×10^3	1.171×10^5	1.92	0.604
0.10	9.07×10^3	1.10×10^5	1.8	0.348
0.20	5.86×10^3	7.06×10^4	1.16	0.026
0.30	5.06×10^3	6.084×10^4	1.0	0.0095

The errors in Table 3 are all positive.

Error due to frequency drift (motor hunting)

The time between successive start pulses of the chopper was measured and found to deviate $\pm5\%$ under the worst possible condition. The following was the method used to determine the frequency change.

$$\theta = \int_{t_o}^{t_1} W(t)dt = \pi \text{ for 1/2 revolution}$$

$$W(t) = W_s + k \sin\pi t$$

$$t = t_1 - t_o$$

$$t \text{ at 100 Hertz} = \frac{\pi \text{ rad}}{100\ \pi \text{ rad/sec}} (1 \pm .05) = 0.01 \pm 0.0005 \text{ sec}$$

$$\theta = \int_{t_o}^{t_1} (\omega_s + k\pi \sin t)dt$$

$$= \omega_s t - \frac{k}{\pi} \cos\pi t \Big|_{o}^{1.05\times10^{-2}}$$

$$= (100\pi)(1.05\times10^{-2}) - \frac{k}{\pi} \cos(1.05\times10^{-2}\pi) + 0 - \frac{k}{\pi}$$

where: ω_s = 100π rad/sec for a power supply frequency of 100 Hertz

t_o = time of peak of first pulse

t_1 = time of peak of next pulse

k = amplitude of fluctuation

For this time interval θ should = π

$$\pi = 1.05\pi - \frac{k}{\pi}(.9946) - \frac{k}{\pi}$$

$$k = 0.248$$

$$\omega(t) = \omega_s + 0.248 \sin\pi t$$

$$= 100\pi \pm 0.248 \text{ for the worst case}$$

$$\omega = \pi f \text{ for 1/2 revolution}$$

$$\Delta f = \pm \frac{0.248}{3.1416} = \pm 0.079 \text{ Hertz}$$

Thus frequencies of 99.921 Hertz and 100.079 Hertz were input to the program. Table C 4 gives the data and differences observed.

Table C 4. Effect of variation in motor frequency

Reference value x 10^{-10} energy (eV)	Observed value x 10^{-10} & energy (eV) for 100.079 Hertz	Observed value x 10^{-10} & energy (eV) for 99.921 Hertz	Difference for 100.079 Hertz	Difference for 99.921 Hertz
39.25	39.25	39.0	0.0	-0.25
0.02	0.02	0.02	0	0
46.4	46.2	46.30	-0.2	-0.1
0.03	0.03	0.03	0	0
48.5	48.25	48.5	-0.25	0
0.04	0.04	0.04	0	0
45.8	45.75	45.90	-0.05	+0.10
0.06	0.06	0.06	0	0
40.5	40.75	40.6	+0.25	+0.10
0.08	0.08	0.08	0	0
33.0	33.20	33.0	+0.20	0
0.10	0.10	0.10	0	0
13.8	14.0	13.9	+0.20	+0.10
0.20	0.20	0.20	0	0
9.75	9.75	9.75	0	0
0.30	0.30	0.30	0	0

Error due to larger effective chopper radius

The chopper was aligned perpendicular to the neutron beam each time by eye. If the chopper was not perpendicular to the neutron beam, the effective radius of the chopper increased. The chopper was aligned many times by eye, and measurements were made to determine the most probable effective radius increase. It was found to be 0.010 inches. Therefore, a value of 1.510 inches was input for R in the computer program to determine its effects. Table C 5 gives the results.

Table C 5. Effect of variation in chopper radius

Reference value x 10^{-10} energy (eV)	Observed value x 10^{-10} & energy (eV) for R = 1.510"	Difference
39.25	40.5	+1.25
0.02	0.0172	-0.0028
46.4	47.0	+0.60
0.03	0.0282	-0.0018
48.5	49.5	+1.0
0.04	0.0390	-0.001
45.8	46.75	+0.95
0.06	0.0596	-0.0004
40.5	40.25	-0.25
0.08	0.0798	-0.002
33.0	32.50	-0.50
0.10	0.10	0
13.8	12.75	-1.05
0.20	0.20	0
9.75	8.75	-1.0
0.30	0.30	0

Possible error due to chopper slit width

The chopper slit width was the vertical height of the window for neutron transmission. It was not known whether there was any error in the value used [12]. However, a small error in the slit width could have caused a large error in the spectrum determined. Upon investigation of the tolerances used in design, and for the materials used, a deviation of $\pm$ 0.0002 inches was applied due primarily to the inherent ripple in the aluminum sheet used for the window. The values of slit width employed for analysis were 0.0202 inches and 0.0198 inches. Table C 6 gives the results.

Based on the data previously derived the variances and standard deviations were calculated. For small deviations in the function and variables, it can be shown that [5],

$$\sigma^2 = \left(\frac{\Delta f}{\Delta a} \sigma_a \right)^2 + \left(\frac{\Delta f}{\Delta b} \sigma_b \right)^2 = \text{---} \left(\frac{\Delta f}{\Delta m} \sigma_m \right)^2$$

Where: σ^2 is the variance

Δf is the change in the function due to the change in the variable

Δa is the deviation of the variable a

σ_a is the standard deviation of a

It was assumed that the distribution of the variable was uniform. The assumption of a uniform distribution is very pessimistic and therefore gives an upper limit of expected error. Thus the variance was of the form [8],

Table C 6. Effect of variation in chopper slit width

Reference value x 10^{-10} & energy (eV)	Observed value x 10^{-10} & energy (eV) for S=0.0202"	Observed value x 10^{-10} & energy (eV) for S=0.0198"	Difference for S=0.0202"	Difference for S=0.0198"
39.25	40.3	37.75	+1.05	-1.50
0.02	0.02	0.02	0	0
46.4	47.25	44.90	+0.85	-1.50
0.03	0.03	0.032	0	+0.002
48.5	49.5	47.0	+1.0	-1.50
0.04	0.04	0.0405	0	+0.0005
45.8	46.8	44.75	+1.0	-1.05
0.06	0.06	0.0602	0	+0.0002
40.5	41.5	39.75	+1.0	-0.75
0.08	0.08	0.0801	0	+0.0001
33.0	33.8	32.5	+0.80	-0.5
0.10	0.10	0.10	0	0
13.8	14.15	13.75	+0.35	-0.05
0.20	0.20	0.20	0	0
9.75	9.82	9.60	+0.07	-0.15
0.30	0.30	0.30	0	0

$$\sigma_a^2 = \frac{(2\Delta a)^2}{12}$$

$$\sigma_a = \left[\frac{(2\Delta a)^2}{12}\right]^{1/2}$$

Where Δa corresponds to the maximum deviation of the variable a, and variables a, b, c, d, and e correspond to time delay, flight path, frequency change, effective chopper radius, and chopper slit width respectively. The contribution to the error from detector dead time was added directly but only to the positive deviation since it yielded a positive deviation.

The standard deviation of the variables is computed below:

$$\sigma_a^2 = \frac{(2\Delta a)^2}{12} = \frac{(2x8.63)^2}{12} = 24.826$$

$$\sigma_b^2 = \frac{(2\Delta b)^2}{12} = \frac{(2x6.47)^2}{12} = 6.07363$$

$$\sigma_c^2 = \frac{(2\Delta c)^2}{12} = \frac{(2x0.079)^2}{2} = 6.07363$$

$$\sigma_d^2 = \frac{(2\Delta d)^2}{12} = \frac{(2x0.01)^2}{12} = 0.333x10^{-4}$$

$$\sigma_e^2 = \frac{(2\Delta e)^2}{12} = \frac{(2x2x10^{-4})^2}{12} = 1.3x10^{-8}$$

Thus the variance in the positive direction (i.e., positive Δf's) at 0.02 eV was:

$$\sigma^2 = \left(\frac{\Delta f}{\Delta a}\sigma_a\right)^2 + \left(\frac{\Delta f}{\Delta b}\sigma_b\right)^2 + \left(\frac{\Delta f}{\Delta c}\sigma_c\right)^2 + \left(\frac{\Delta f}{\Delta d}\sigma_d\right)^2 + \left(\frac{\Delta f}{\Delta e}\sigma_e\right)^2$$

$$= \left(\frac{0.25\times10^{10}\times4.98}{8.63}\right)^2 + 0 + 0 + \left(\frac{1.25\times10^{10}\times0.5774\times10^{-2}}{10^{-2}}\right)^2$$

$$+ \left(\frac{1.05\times10^{10}\times1.14\times10^{-4}}{2.0\times10^{-4}}\right)^2$$

$$\sigma^2 = 0.89912 \times 10^{20}$$

Therefore, the standard deviation σ was $\sigma = 0.9486\times10^{10}$. The dead time error was added directly. Thus the final σ was $(0.9486 + 0.0576) \times 10^{10} = 1.00624 \times 10^{10}$.

The variance in the negative direction at 0.02 eV was:

$$\sigma^2 = \left(\frac{0.40\times10^{10}\times4.98}{8.63}\right)^2 + \left(\frac{0.75\times10^{10}\times0.2714}{0.47}\right)^2$$

$$+ \left(\frac{0.40\times10^{10}\times0.2714}{0.47}\right)^2 + \left(\frac{0.25\times10^{10}\times0.0456}{0.79}\right)^2$$

$$+ \left(\frac{1.50\times10^{10}\times1.14\times10^{-4}}{2\times10^{-4}}\right)^2$$

$$= 0.0533\times10^{20} + 0.18756\times10^{20}\times0.05335\times10^{20} + 0.02082\times10^{20}$$

$$+ 0.731\times10^{20} = 1.046\times10^{20}$$

Thus the standard deviation σ was equal to 1.02276×10^{10}.

Table C 7 gives the standard deviation at each energy and the resultant percent error. The values of standard deviation given in the table are plotted in Figure 30.

In some cases the spectrum was observed to have devia-

Table C 7. Estimates of uncertainty in measured values of intensity as a function of energy

Energy (eV)	Reference value x 10^{-10}	plus x 10^{-10}	minus x 10^{-10}	% error plus	% error minus
0.02	38.25	1.00624	1.02276	2.56	2.6
0.03	46.4	0.878	0.9837	1.9	2.12
0.04	48.5	1.336	0.9752	2.75	2.0
0.06	45.8	1.55	0.613	3.38	1.34
0.08	40.5	1.278	0.4865	3.15	1.2
0.10	33.0	0.84	0.378	2.55	1.45
0.20	13.8	0.31614	0.6077	2.29	4.4
0.30	9.75	0.0595	0.585	0.61	6.0

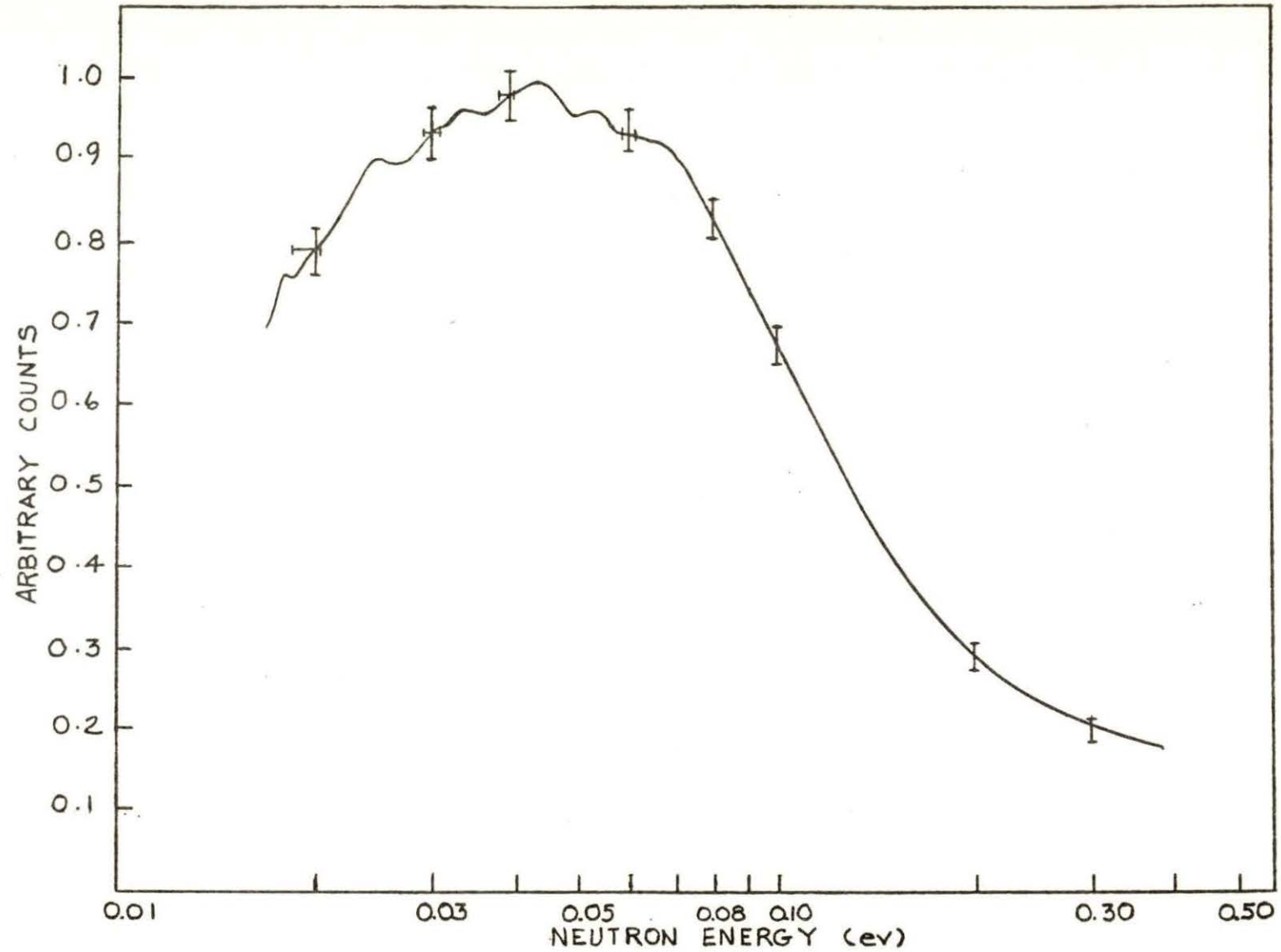

Figure 30. Reference energy spectrum with typical error ranges

tions in the energy for deviations in the variables. Based on the data previously derived, the variances and standard deviation were calculated. The method used was the same as previously illustrated.

The energy variance in the positive direction at 0.02 eV was:

$$\sigma^2 = \left(\frac{2.5\times10^{-4}\times4.98}{8.63}\right)^2 + \left(\frac{3.5\times10^{-4}\times0.2714}{0.47}\right)^2$$

$$\sigma^2 = 2.081\times10^{-8} + 4.085\times10^{-8}$$

$$\sigma^2 = 6.166\times10^{-8}$$

Therefore: $\sigma = 2.483\times10^{-4}$

The energy variance in the negative direction at 0.02 eV was:

$$\sigma^2 = \left(\frac{3\times10^{-4}\times4.98}{8.63}\right)^2 + \left(\frac{0.28\times10^{-2}\times.5774\times10^{-2}}{0.01}\right)^2$$

$$\sigma^2 = 2.997\times10^{-8} + 261.4\times10^{-8}$$

$$\sigma^2 = 264.375\times10^{-8}$$

Therefore: $\sigma = 16.26\times10^{-4}$

Table C 8 gives the standard deviation in energy at each energy, and the resultant percent error.

The values of the standard deviation in Table C 8 are illustrated in Figure 30.

Table C 8. Estimates of uncertainty in measured values of energy as a function of energy

Energy (eV)	σ plus x 10^4	σ minus x 10^4	% error plus	% error minus
0.02	2.483	16.26	1.24	8.13
0.03	11.59	10.49	3.86	3.5
0.04	3.34	5.89	0.84	1.5
0.06	1.555	2.38	0.26	0.4
0.08	0.817	1.115	0.1	0.144
0.10	0.0	0.0	0	0
0.20	0.0	0.0	0	0
0.30	0.0	0.0	0	0

APPENDIX D. CALCULATION OF EXPECTED NEUTRON ENERGIES AND RELATIVE MAGNITUDE WHICH WILL BE SCATTERED BY POLYCRYSTALLINE ALUMINUM

The following illustrates how the expected scattering energies and relative magnitudes were calculated for polycrystalline aluminum.

The aluminum unit cell is a face-centered cubic. For a cubic structure the relative intensity of coherent scattering of the planes is $3!x2^n/K$ [9]. In the preceding equation n equals the number of non-zero indices and K equals the number of like indices (e.g., for a 1,1,1 plane K = 3). For the 1,1,1 plane the relative intensity equals $6x2^3/3 = 16$. However, the smallest relative intensity obtained was six. Therefore, the others were normalized to six. Thus, the 1,1,1 plane has a normalized relative intensity of 2.67.

The following was used to determine the energies of the neutrons at which the scattering will occur: $\lambda = 2d\sin\theta$ where the distance d between scattering planes is $a/\sqrt{h^2+k^2+\ell^2}$ where a is the lattice constant (4.04145 Å for aluminum), and h, k, ℓ are the indices of the plane, and λ is the wave-length associated with the neutron. Thus

$$\lambda = \frac{2a \sin\theta}{h^2+k^2+\ell^2} .$$

The only cases of interest are for values of θ such that $\sin\theta = 1$ (i.e., $\lambda = \frac{2a}{h^2+k^2+\ell^2}$). For the 2,2,2 plane

$$\lambda = \frac{(2)(4.04145\text{Å})}{(2^2+2^2+2^2)^{1/2}} = 2.335\text{Å}.$$

The energy of a neutron with wave-length $\lambda(\text{Å})$ is $E = \left(\frac{0.286}{\lambda(\text{Å})}\right)^2$ electron volts. Thus for the 2,2,2 plane $E = \left(\frac{0.286}{2.335\text{Å}}\right)^2 =$ 0.015 electron volts.

From Figure 11 it can be seen that for neutron energies approximately 0.08 electron volts and higher, the irregularities in the spectrum are no longer observed. The reason for this is that the scattering energies are so close together that the individual scattering effects are no longer distinguishable. Table C 1 lists the scattering planes in aluminum, their normalized relative intensity, and the energy of the neutrons which will be scattered by this plane.

Table D 1. Relative intensity of diffracted neutron beam as a function of scattering plane orientation

Observed scattering planes in aluminum	Normalized relative intensity	Neutron energy coherently scattered (electron volts)
222	2.67	0.015
400	1.0	0.02
331	4.0	0.0238
420	4.0	0.025
422	4.0	0.0302
511	4.0	0.0333
333	2.67	0.0337
440	2.0	0.04
531	8.0	0.0439
442	4.0	0.0451
600	1.0	0.0451
620	4.0	0.05
533	4.0	0.0537
622	4.0	0.0552
444	2.67	0.0601
551	4.0	0.0625
711	4.0	0.0625